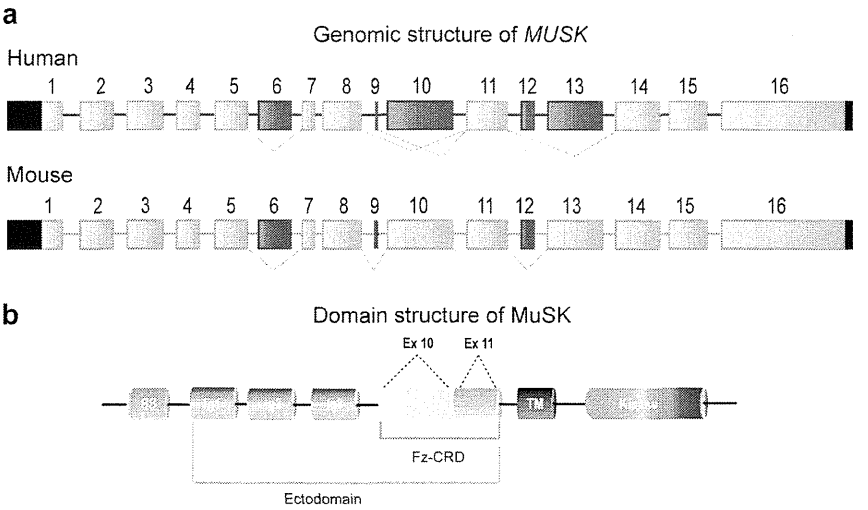

Figure 1 | Structures of human and mouse MuSK. (a) Genomic structures of human *MUSK* and mouse *Musk* genes. Constitutive and alternative exons are shown in green and red boxes, respectively. Black boxes indicate untranslated regions (UTRs) and thin lines indicate introns. Alternative skipping of exons annotated in ENSEMBL 76 are shown by blue connecting lines. (b) Domain structure of MuSK. Fz-CRD is a Wnt-responsive domain encoded by exon 10 coding for 6 cysteines (light blue-colored region of Fz-CRD) and exon 11 coding for 4 cysteines (yellow-colored region of Fz-CRD) in human. SS, signal sequence; TM, transmembrane domain.

and induce AChR clustering, which requires LRP4, but not agrin[16]. In another study, Wnt4 has been shown to induce MuSK phosphorylation by interacting with Fz-CRD in COS7 and HEK293T cells and Wnt4 facilitates mouse NMJ formation *in vivo*[17]. Muscle prepatterning in zebrafish is also facilitated by interaction of Wnt11r with Fz-CRD of a MuSK homolog, *unplugged*[18], which is mediated by enhancing endocytosis of MuSK[19]. In zebrafish, *unplugged*/MuSK has three splice variants: SV1 lacks Ig-like domains 1 to 3 but retains Fz-CRD, and is not responsive to agrin; SV2 lacks Fz-CRD and is not responsive to Wnt; and the full-length isoform that can respond to both agrin and Wnt[18]. Subsequent studies revealed that agrin-non-responsive SV1 is expressed in embryos, which is substituted for by the full-length isoform in adults[18,20,21]. MuSK Fz-CRD additionally plays an important role in motor nerve axon guidance in pathfinding in zebrafish[20,21]. Partial deletions of Fz-CRD have been analyzed in quail QT-6 fibroblasts[22]. Artificial deletion of 6 Fz-CRD cysteines or 4 Fz-CRD cysteines caused lack of an activity for MuSK-rapsyn co-clustering[22]. Amino acids 760 to 820 in the cytoplasmic domain of MuSK, however, have later been shown to be sufficient to confer interaction with rapsyn[23]. As Fz-CRD is an important and obligatory domain of MuSK for Wnt-mediated AChR clustering in zebrafish[18–21] and mouse C2C12 myotubes[16,17], the two discordant reports in zebrafish[22,23] may indicate that Fz-CRD has an additional enhancing effect on MuSK-rapsyn interaction or plays another role in Wnt-mediated AChR clustering. Considering the functional significance of 10 cysteines in Fz-CRD, we humans are likely to have acquired an evolutionally novel Wnt-insensitive MuSK isoform lacking 6 essential cysteines, but the underlying mechanisms of alternative skipping of *MUSK* exon 10 remain unknown.

HnRNP C is a nuclear RNA-binding protein that associates with nascent mRNA transcripts, which plays roles in pre-mRNA splicing[24], mRNA stability[25], and translational modulation[26]. HnRNP C has recently been identified as a molecular ruler to classify RNA polymerase II transcripts for export into two categories: a long mRNA and a short uridine-rich small nuclear RNA (U snRNA)[27]. The Y box-binding protein (YB-1) is a member of the cold shock domain (CSD) protein family, which has binding specificity for both DNA and RNA. YB-1 has multiple roles including transcriptional regulation, translational control, DNA repair, and pre-mRNA splicing[28,29]. HnRNP L is another nuclear RNA-binding protein and a global splicing regulator[30–38]. It also functions in polyadenylation and mRNA stability[39,40].

In the present study, we have dissected the underlying mechanisms of alternative splicing of human *MUSK* exon 10. We first characterized splicing regulatory *cis*-elements by scanning mutagenesis. We then identified that the alternative skipping of *MUSK* exon 10 is coordinately modulated by binding of three splicing suppressors (hnRNP C, YB-1, and hnRNP L) to an exonic splicing silencer (ESS) that is unique to human *MUSK* exon 10. Remarkably, hnRNP C is the master regulator in this regulatory process, and YB-1 and hnRNP L have additive effects to efficiently achieve splicing suppression.

Results

Alternative splicing of *MUSK* exon 10 is unique to human. Since exons 9 (7 nucleotides) and 10 (264 nucleotides) of human *MUSK* are alternatively spliced according to the gene annotation databases, we initially examined the differential selection of these two exons in human skeletal muscle. Using total RNA isolated from human skeletal muscle (Clontech), fragments spanning exons 8 to 11 were amplified by RT-PCR (Fig. S2d). Sequencing of the RT-PCR products revealed three splicing isoforms: (i) exons 9 and 10 included; (ii) exon 10 skipped; and (iii) exons 9 and 10 skipped (Fig. S2f). We could not detect any transcript that skipped only exon 9. We also performed a similar experiment using total RNA isolated from immortalized human myogenic KD3 cells and primary human myoblasts (SkMC), and obtained similar results (Fig. S2d and f). The three observed splicing isoforms are not correctly mapped to the human genome in UCSC Genes, RefSeq, ENCODE/GENCODE Ver. 19 and H-Inv ver. 8.3. As cDNA sequences registered in these annotation databases are correct, a short exon 9 that is comprised of only 7 nucleotides is likely to have precluded correct mapping of cDNAs to the human genome. We also confirmed lack of alternative splicing of mouse *Musk* exon 10 in 10 different skeletal muscle tissues as well as in C2C12 mouse myoblasts (Figs. S2e and S7c). Lack of alternative splicing of mouse *Musk* exon 10 is correctly annotated in all of the gene annotation databases shown above. In this study, we investigated the underlying mechanisms of alternative skipping of exon 10 unique to human.

Construction of minigenes for splicing analysis. We first constructed a human *MUSK* minigene in pcDNA3.1D/V5/His-TOPO expression vector (Invitrogen) spanning exons 8 to 11 (Fig. 2a). Exon 10 in the pcDNA3.1 minigene was alternatively spliced in HeLa cells,

as we observed in human skeletal muscle. We next inserted exon 10 and flanking intronic sequences (245 nucleotides in the upstream intron and 200 nucleotides in the downstream intron) into the modified exon-trapping vector pSPL3[41], which carried two proprietary constitutive exons on each end (Fig. S3a). The pSPL3-human-*MUSK* minigene (H-iE10i) successfully recapitulated alternative splicing of exon 10 in HeLa cells (Fig. S3a). Serial deletions of intronic nucleotides from both ends of H-iE10i revealed that the shortest minigene (H-iE10i-Δ6) that carried 100 nucleotides in the upstream intron and 60 nucleotides in the downstream intron was still alternatively spliced like H-iE10i in HeLa cells (Fig. S3a). This minigene was termed pSPL3-human-*MUSK* (pH-wt) (Fig. 2b) and used in the subsequent experiments.

We also constructed a similar minigene harboring mouse exon 10 and flanking intronic sequences, pSPL3-mouse-MuSK (pm-wt), and found that exon 10 is constitutively included in this minigene in HeLa cells (Fig. 2b). As the mouse minigene was not alternatively spliced even in human cells, we assumed that nucleotides unique to human enabled alternative splicing of exon 10. We confirmed that our minigene was similarly alternatively spliced in KD3 cells and HeLa cells (Fig. 2a and b). Due to better transfection efficiency, we used HeLa cells and pH-wt/pm-wt in the following studies.

Identification of two exonic splicing silencer (ESS) blocks in human exon 10. We next searched for exonic/intronic segments carrying splicing *cis*-elements in pH-wt. To this end, we constructed chimeric minigenes made of variable combinations of human and mouse segments (Fig. 2c). We found that the introduction of mouse exon 10 into pH-wt resulted in constitutive splicing (pH-EC in Fig. 2c). We next introduced the first or second

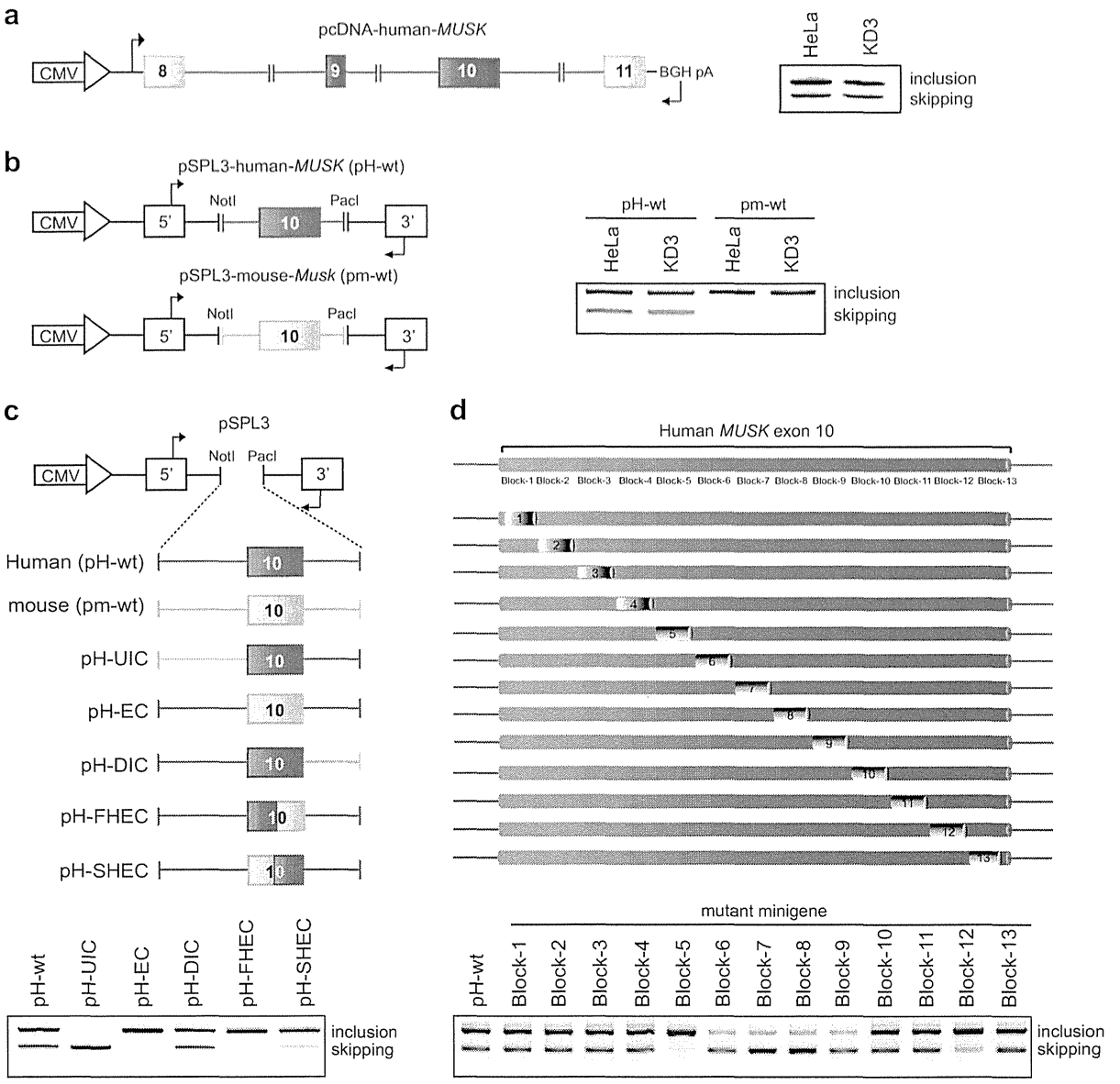

Figure 2 | Construction of minigenes and systematic identification of splicing regulatory *cis*-elements. (a) Structure of human *MUSK* minigene in pcDNA3.1D vector (pcDNA-human-*MUSK*). RT-PCR of this minigene in HeLa and KD3 cells are shown at right. Alternatively and constitutively spliced regions are shown in red and green, respectively. (b) Structure of pSPL3 minigene harboring *MUSK/Musk* exon 10 and flanking introns originated from human (pSPL3-human-*MUSK*, termed pH-wt) and mouse (pSPL3-mouse-*Musk*, termed pm-wt). RT-PCR of these minigenes in HeLa and KD3 cells are shown at right. (c) Schematic of chimeric constructs of pSPL3-human-*MUSK* minigene partially replaced by corresponding mouse sequences shown in green. RT-PCR of each chimeric minigene in HeLa cells is shown below. (d) Schematic of *cis*-regulatory block-scanning mutagenesis of *MUSK* exon 10 in the context of pSPL3-human-*MUSK* (pH-wt) minigene. A 20-nucleotide heterologous sequence of 5′-TCAGTATGACTCTCAGTATG-3′ is introduced into each block. RT-PCR of pH-wt and 13 block-mutant minigenes in HeLa cells are shown bellow. Arrows point to primer positions in (a), (b), and (c).

half of mouse exon 10 into pH-wt, and found that both constructs resulted in constitutive splicing (pH-FHEC and pH-SHEC in Fig. 2c). To specifically identify exonic splicing *cis*-elements, we sequentially introduced a 20-nucleotide heterologous sequence block (5′-TCAGTATGACTCTCAGTATG-3′), which was previously reported to have no effect on splicing[37,42] (Fig. 2d). We scanned the entire exon 10 by substituting 13 blocks excluding the first and last three nucleotides of the exon. The block scanning mutagenesis detected a potential ESS in two separate blocks (blocks 5 and 12) and a potential exonic splicing enhancer (ESE) in four consecutive blocks (blocks 6, 7, 8, and 9) (Fig. 2d). As skipping of exon 10 has a prospective inhibitory effect on AChR clustering, we dissected the mechanisms associated with ESSs in this communication.

Dissection of ESS blocks on a nucleotide level and detection of *trans*-acting factors. We next dissected the identified ESS blocks on a nucleotide level. Alignment of human and mouse blocks 5 (ESS5) and 12 (ESS12) revealed three and two discordant nucleotides, respectively. Artificial introduction of discordant nucleotides into ESS5 (pH-mB5) and ESS12 (pH-mB12) resulted in profound and moderate loss of exon skipping, respectively (Fig. 3a and b), which were consistent with the block-scanning mutagenesis experiments (Fig. 2d). Therefore, the splicing suppressive effect of ESS5 was stronger than that of ESS12.

The vast majority of splicing enhancer and silencer sequences have been reported to function through the binding of cognate regulatory proteins[43]. To determine if potential *trans*-acting factors stably interact with the ESS sequences, binding reactions were performed with a HeLa nuclear extract and an RNA probe harboring human or mouse ESS5 sequence (Fig. 3c). An RNA mobility shift assay with a native gel showed three slow migrating complexes with the ^{32}P-labeled human ESS5 RNA probe (H-B5) (Fig. 3d). In contrast, the two slow migrating complexes observed with H-B5 were not visible with the mouse ESS5 RNA probe (m-B5). We also performed a similar experiment with human/mouse ESS12 RNA probes, but could not detect any differentially associated complex (Fig. S3b and c). We thus focused on identification of the proteins bound to ESS5.

HnRNP C, YB-1, and hnRNP L are bound to human ESS5. We next performed an RNA affinity purification assay using a HeLa nuclear extract and a biotinylated ESS5 RNA probe (Fig. 3c). Three distinct bands of ~70, ~50, and ~40 kD were associated with the wild-type human ESS5 RNA probe (H-B5) but not with the mouse probe (m-B5) or a partially deleted human probe (H-B5Δ5) (Fig. 3e). Mass spectrometry analysis of the excised bands disclosed that the identified bands were hnRNP L, YB-1, and hnRNP C, respectively, which were confirmed by immunoblotting using respective antibodies [anti-hnRNP L 4D11 (sc-32317, Santa Cruz Biotechnology), anti-YB1 (A303-230A, Bethyl Laboratories), and anti-hnRNP C1/C2 4F4 (SC-32308, Santa Cruz Biotechnology)] (Fig. 3f). Similar analysis with ESS12 detected no differentially associated molecule (Fig. S3d).

HnRNP C, YB-1, and hnRNP L coordinately enhance skipping of human *MUSK* exon 10. We next examined the effects of the identified *trans*-factors on skipping of exon 10 by siRNA-mediated downregulation of the individual factors in HeLa cells. We first confirmed efficient downregulation of each factor (Fig. 4a). Downregulation of hnRNP C resulted in a significant loss of exon skipping (Fig. 4b). Similarly, downregulation of YB-1 and hnRNP L caused a loss of exon skipping, but to a lesser extent compared to hnRNP C. Downregulation of all three *trans*-factors exerted a more prominent effect than hnRNP C alone. Thus, YB-1 and hnRNP L are likely to have additive effects on exon skipping. We observed similar alterations in alternative splicing patterns with a second set of siRNAs targeting different sites of each mRNA (Fig. S3e).

We next overexpressed cDNA of each *trans*-factor in HeLa cells. We first confirmed the expression of each cDNA by immunoblotting (Fig. 4c). As expected, overexpression of hnRNP C induced skipping of exon 10 (Fig. 4d). A similar increase in exon skipping was also observed with overexpression of YB-1 and hnRNP L, but to a lesser extent compared to hnRNP C. The most prominent skipping was observed when all three factors were overexpressed together, which was consistent with the knockdown results.

HnRNP C is a critical regulator in inducing exon skipping, whereas YB-1 and hnRNP L have augmenting effects. Having identified the critical *cis*-element and their cognate-binding partners, we next analyzed the molecular basis of specific binding of each *trans*-factor to ESS5. HnRNP C prefers to bind to poly-T stretch motifs[24,44] and both hnRNP L and YB-1 prefer to bind to C/A-rich motifs[29,32,45]. ESS5 carries a stretch of five T's in the first half of the block and a C/A-rich sequence in the second half of the block (H-B5 in Fig. 5a and b). *In vitro* SELEX studies of hnRNP L demonstrated that CACA and ACAC sequences confer high-affinity binding motifs and that CAAC and CACC confer low-affinity binding motifs for hnRNP L[32], where motifs present in ESS5 are underlined. On the contrary, *in vitro* SELEX studies of YB-1 revealed that CATC and CACC sequences confer high-affinity binding motifs for YB-1[29], where a motif present in ESS5 is underlined. Therefore, the second half of ESS5 harbors overlapping binding motifs of both YB-1 and hnRNP L. To characterize the precise binding sites of the associated factors, we introduced a series of artificial point mutations into the human ESS5 RNA probe and checked the binding of each factor by RNA-affinity purification followed by Western blotting (Fig. 5a and b). We observed that poly-T stretch-disrupting mutations in the first half indeed abolished the binding of hnRNP C (Fig. 5a, lanes 3, 4, and 5), and four or more consecutive T-nucleotides are necessary for hnRNP C binding. To our surprise, we noticed that binding of YB-1 and hnRNP L was also compromised along with disruption of the hnRNP C binding (Fig. 5a, lanes 3, 4 and 5). This suggested that binding of YB-1 and hnRNP L was dependent on poly T-stretch. On the other hand, introduction of mutations in the second half (C/A-rich sequences) compromised binding of YB-1 and hnRNP L, but not of hnRNP C (Fig. 5b). In addition, characterization of essential nucleotides for binding of hnRNP L (CAACA) and YB-1 (ACACCT) revealed that binding motifs of hnRNP L and YB-1 indeed overlap (CAACACCT) in the second half of ESS5, where the overlapping nucleotides are underlined. Considering the overall findings (Fig. 5c), we predicted that binding of hnRNP C to the poly-T stretch facilitates the binding of YB-1 and hnRNP L to the adjacent downstream site. To test this hypothesis, we depleted hnRNP C from a HeLa nuclear extract using a specific antibody (Fig. S4a) and performed RNA affinity purification assays. As we had expected, depletion of hnRNP C nullified the binding of YB-1 and hnRNP L (Fig. S4b).

Binding of hnRNP C, YB-1, and hnRNP L to ESS5, but not to the other site, induces skipping of *MUSK* exon 10. Having characterized a coordinated regulation of hnRNP C, YB-1, and hnRNP L on skipping of exon 10, we next examined the additive effect of YB-1 or hnRNP L on hnRNP C-mediated exon skipping. To this end, we made a reporter minigene (pSPL3-human-*MUSK*-MS2-PP7), in which the bacteriophage MS2 coat protein-binding site was substituted for the native 'TTTTTCT' sequence in the first half of ESS5 (the binding site of hnRNP C), and the bacteriophage PP7 coat protein-binding site was substituted for the native 'CAACACCTC' sequence in the second half of ESS5 (the binding site of YB-1 and hnRNP L) (Fig. 5d). We also made cDNA fusion constructs, hnRNP C-MS2, YB-1-PP7, and hnRNP L-PP7, to artificially tether splicing *trans*-factors to the respective sites. As expected, tethering of MS2-tagged hnRNP C alone efficiently induced exon skipping of 79%

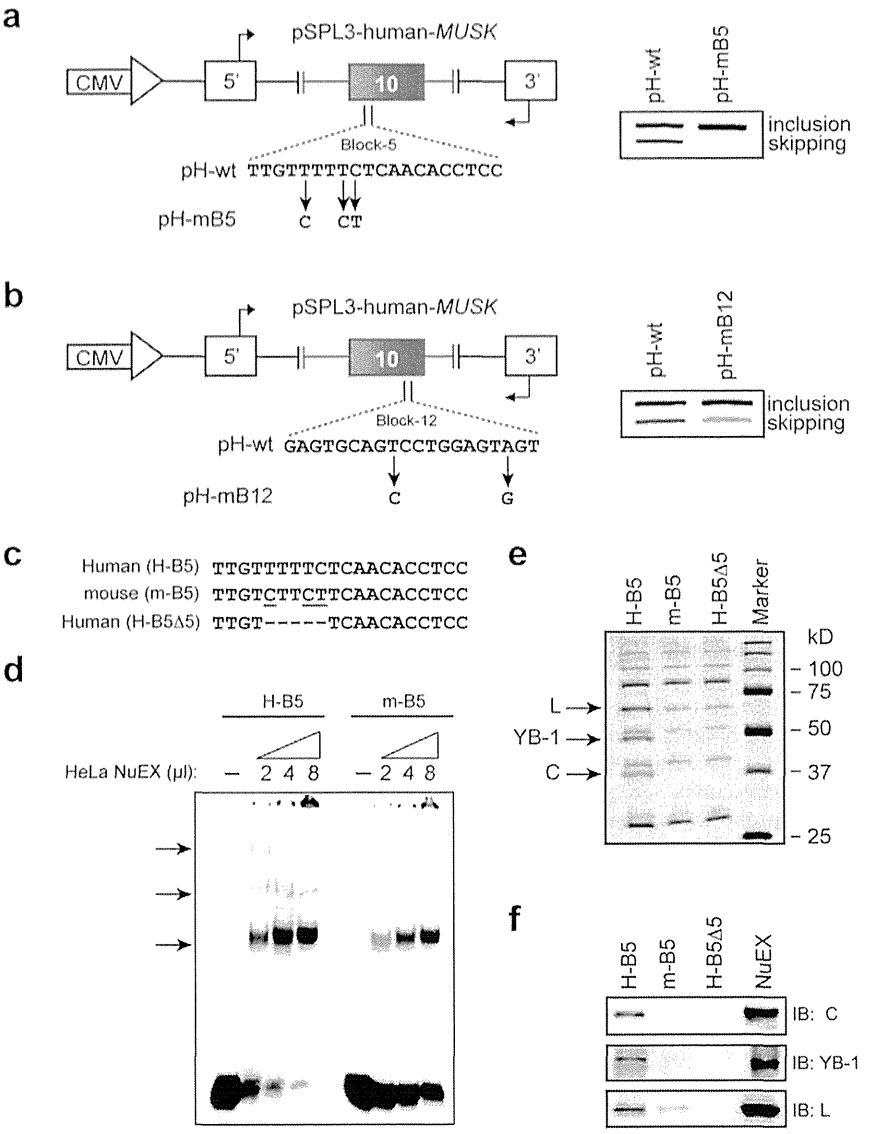

Figure 3 | HnRNP C, YB-1 and hnRNP L bind to exon 10 of human *MUSK*. (a, b) Mouse nucleotides are introduced into ESS5 (a) and ESS12 (b) of pH-wt to generate pH-mB5 and pH-mB12, respectively. RT-PCR of each mutated minigene in HeLa cells is compared with that of pH-wt. Primer positions are shown by arrows. (c) Sequences of ESS5 RNA probes carrying human (H-B5), mouse (m-B5), and partially deleted (H-B5Δ5) sequences. (d) ^{32}P-labeled H-B5 or m-B5 RNA probe was incubated in the presence or absence of HeLa nuclear extract (NuEX) and resolved on a native polyacrylamide gel to observe free and protein-bound RNA species (arrows). (e) Coomassie blue staining of RNA affinity-purified products from HeLa nuclear extract using the indicated biotinylated RNA probes. Three proteins of ~70, ~50, and ~40 kDa (arrows) are differentially associated with H-B5 compare to m-B5 and H-B5Δ5. Mass spectrometry analysis revealed that the three proteins are HnRNP L (L), YB-1, and hnRNP C (C). (f) Immunoblotting (IB) of RNA affinity purified proteins in panel (e) with the indicated antibodies.

(Fig. 5e, lane 3). Tethering of PP7-tagged YB-1 and hnRNP L without tethering MS2-tagged hnRNP C induced exon skipping of 52% (Fig. 5e, lane 5) and 36% (Fig. 5e, lane 8), respectively. In contrast, hnRNP C, YB-1, or hnRNP L without a tethering tag did not induce exon skipping (Fig. 5e, lanes 2, 4 and 7), suggesting that ESS5 was the only site where these factors were able to bind and function. We also confirmed that MS2- or PP7-tagged factor has no effect on a minigene lacking MS2- or PP7-binding site (Fig. S4d). Simultaneous recruitment of hnRNP C with either YB-1 or hnRNP L further induced exon skipping (Fig. 5e, lanes 6 and 9), which reconfirmed the additive effects of YB-1 and hnRNP L on hnRNP C-mediated splicing suppression.

RNA-dependent interaction of hnRNP C, YB-1, and hnRNP L and search for similar targets in other human genes. We next examined the molecular interaction between the three *trans*-factors. Co-immunoprecipitation revealed that HnRNP C and hnRNP L were bound in an RNA-dependent manner (Fig. S5a), whereas hnRNP C and YB-1 were not (Fig. S5b). Similarly, hnRNP L and YB-1 were bound in an RNA-dependent manner (Fig. S5c), which was consistent with a previous report[45].

We further asked if coordinated splicing regulation by hnRNP C, YB-1, hnRNP L is unique to *MUSK* exon 10. As hnRNP L has highly degenerative SELEX motifs, which are overlapping with YB-1 motifs, we analyzed coordinated splicing only by hnRNP C and YB-1. Search for adjacent hnRNP C- and YB-1-binding motifs in human alternative cassette exons and flanking introns detected 378 candidate sites. We randomly selected 37 exons and analyzed alternative splicing in HeLa cells in the presence of siCont, siC, siYB-1, and siC/siYB-1. We found that alternative splicing events of 9 exons were affected by hnRNP C and/or YB-1 in HeLa cells, whereas 13 exons were not expressed and 15 exons were not alternatively spliced or affected

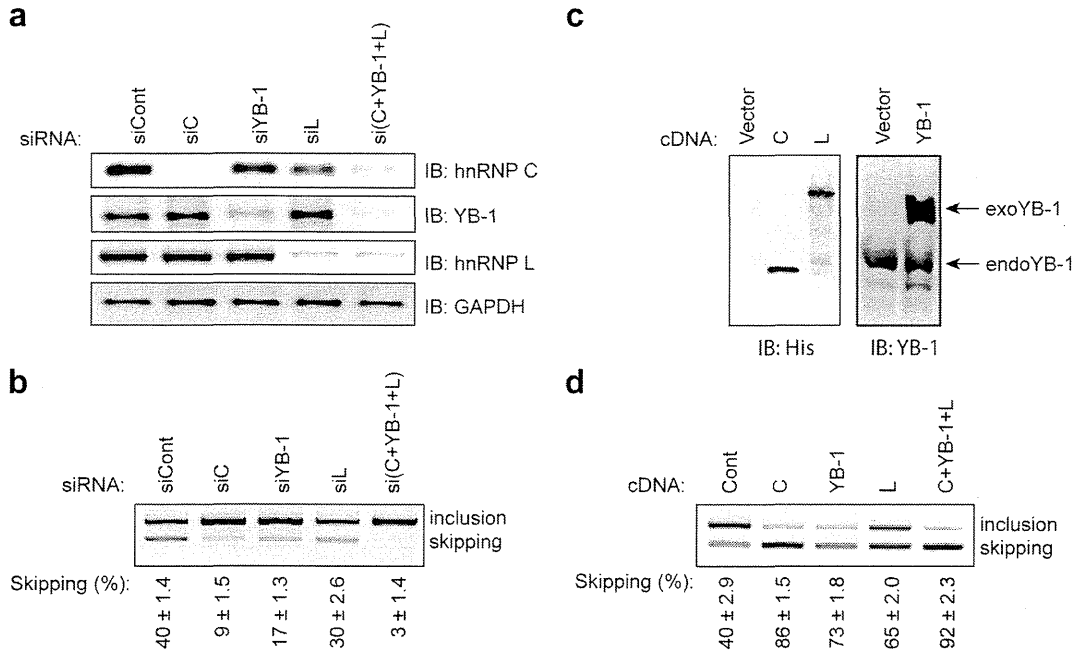

Figure 4 | HnRNP C, YB-1, and hnRNP L coordinately promote skipping of *MUSK* exon 10. (a) Immunoblotting (IB) using the indicated antibodies after gene knockdown with siRNA against control (siCont), hnRNP C (siC), YB-1 (siYB-1), and hnRNP L (siL) in HeLa cells. (b) RT-PCR of pSPL3-human-*MUSK* (pH-wt) minigene in HeLa cells treated with the indicated siRNAs. The mean and SD (n = 3) of the ratio of exon skipping in each treatment is shown below the gel image. (c) Immunoblotting (IB) with the indicated antibodies after cDNA overexpression of hnRNP C, YB-1, and hnRNP L in HeLa cells. Endogenous (endo) and exogenous (exon) YB-1 proteins are pointed by arrows. (d) RT-PCR of pH-wt minigene in HeLa cells co-transfected with the indicated cDNAs. The mean and SD (n = 3) of the ratio of exon skipping in each treatment is shown below the gel image.

by knockdown (Fig. S6). Among the 9 exons, 3 exons were coordinately skipped by hnRNP C and YB-1 (Fig. S6a).

Expressions of splicing repressing hnRNP C and YB-1 are reduced with muscle differentiation. As MuSK is a muscle-specific receptor protein having an important role in muscle development and function, we next examined the splicing profile of human *MUSK* exon 10 in different stages of myogenic differentiation. We cultured immortalized human myogenic KD3 cells in differentiation medium for four days to make myotubes (Fig. 6a). RT-PCR spanning endogenous *MUSK* exon 10 at different time points revealed that skipping of exon 10 was suppressed on and after differentiation day 3 (Fig. 6b, and Supplementary Table 1). Similarly, myotube differentiation suppressed skipping of *MUSK* exon 10 in primary human myoblasts (SkMC) (Figs. S7a, b, and 6c), and skipping of exon 10 constitutes only 12% in human skeletal muscle (Fig. 6c and Supplementary Table 1). Thus, skipping of exon 10 is a minor event in any differentiation stages of myogenic and muscle cells.

In KD3 cells, we found that the expressions of hnRNP C and YB-1 were indeed decreased on and after day 3, whereas the expression level of hnRNP L was not significantly changed at the mRNA (Fig. 6d) and protein (Fig. 6e) levels. Therefore, reduction of hnRNP C and YB-1 in the course of muscle differentiation causes reduction of skipping of human *MUSK* exon 10 to produce a Wnt-sensitive MuSK isoform.

Discussion

In this study, we have identified splicing regulatory *cis*-elements and cognate *trans*-factors that drive alternative splicing of human *MUSK* exon 10. HnRNP C enhances exon skipping in coordination with YB-1 and hnRNP L by binding to a regulatory exonic splicing silencer, ESS5. Two splicing suppressive *cis*-elements, ESS5 and ESS12, are recognized by block-scanning mutagenesis, although the ESS activity of ESS12 is not as conspicuous as that of ESS5. Most splicing regulatory ESSs and ESEs function through the binding of cognate regulatory proteins[43]. Indeed, ESS5 is recognized by the three splicing *trans*-factors, but no associated molecules are detected for ESS12. In contrast, the splicing suppressive activity of ESS12 is likely to be regulated by a local secondary structure of pre-mRNA. Alternatively, a binding affinity of a splicing *trans*-factor to ESS12 is too low to be detected by the RNA mobility shift assay and the RNA affinity purification assay.

We have characterized the mutual coordination between the three *trans*-factors. HnRNP C binds to a poly-T stretch in the first half of ESS5, whereas binding motifs of hnRNP L and YB-1 are overlapped in the second half of ESS5. In addition, binding of YB-1 and hnRNP L is dependent on hnRNP C. One possible mechanism for this is that overlapping binding motifs between hnRNP L and YB-1 provoke competitive binding of the two factors. A third molecule, hnRNP C, may rearrange RNA conformation to stabilize the binding of either hnRNP L or YB-1. Similar RNA-mediated stabilization of binding of another RNA-binding protein by a specific RNA-binding protein has been reported in other genes. In *CD45*, hnRNP L stabilizes the binding of hnRNP A1 in exon 4, in which binding of hnRNP A1 and the subsequent splicing suppression is dependent on hnRNP L[34]. The authors demonstrate that hnRNP L interacts with hnRNP A1, which is lost by RNase. In *Tpm1*, splicing of exon 3 is coordinately repressed by PTB and Raver 1[46]. Interaction between PTB and Raver 1, which requires the target RNA, results in a conformational change of the tertiary complex to bring the repressor domain of both molecules in close apposition to synergistically promote exon skipping. Therefore RNA-dependent molecular interaction and coordinated splicing suppression is unlikely to be unique to ESS5 and is likely to be functional in many other alterative splicing events.

Binding of YB-1 and hnRNP L to the same target and the subsequent coordinated splicing regulation have been previously reported[45]. The authors report that overexpression and depletion of either YB-1 or hnRNP L is sufficient to repress and derepress splicing, respectively. In their report, YB-1 exerts a stronger effect

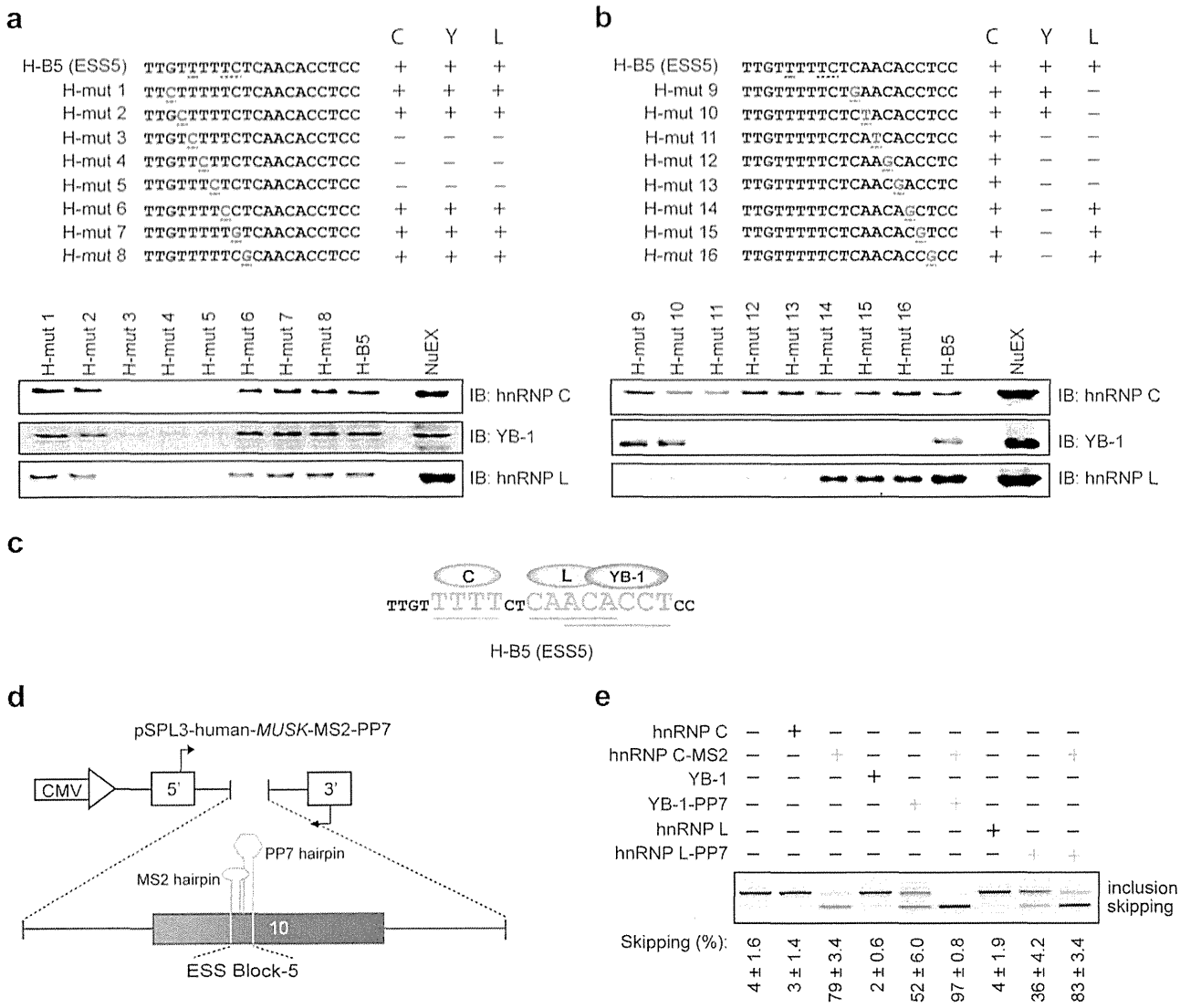

Figure 5 | Binding of hnRNP C, YB-1, and hnRNP L to specific motifs enhances coordinated skipping of *MUSK* exon 10. (a, b) Scanning mutagenesis to map the binding motifs of hnRNP C, YB-1, and hnRNP L in ESS5 (H-B5). RNA probe sequences are shown in the upper panels, where discordant nucleotides between human and mouse are underlined in H-B5 (ESS5). Artificial mutations are shown in red. RNA affinity-purified products are detected by immunoblotting in the lower panels. The results are indicated on the right side by "+" and "−" for positive and negative binding to each probe, respectively. (c) The resulting binding site of each factor from panels (a) and (b) is schematically shown. Essential binding nucleotides are indicated by large green letters and are underlined. (d) Schematic of a reporter minigene (pSPL3-human-*MUSK*-MS2-PP7). MS2 coat protein-binding hairpin RNA (blue) is substituted for the first half of ESS5 (binding site of hnRNP C). Similarly, PP7 coat protein-binding hairpin RNA (orange) is substituted for the second half of ESS5 (binding sites of hnRNP L and YB-1). (e) RT-PCR of pSPL3-human-*MUSK*-MS2-PP7 minigene in HeLa cells that are co-transfected with the indicated effectors. Blue and orange letters match to those in (d). The mean and SD ($n = 3$) of the ratio of exon skipping in each treatment is shown below the gel image.

than hnRNP L, as in our *MUSK* exon 10. To the best of our knowledge, *MUSK* exon 10 is the first target where coordinated splicing regulation by YB-1 and hnRNP L is dependent on hnRNP C. RT-PCR analysis of 37 targets, where an hnRNP C-binding 'TTTT' motif and a YB-1-binding 'CATC/CACC' motif are adjacent to each other in human alternative cassette exons and flanking introns, revealed three alternative cassette exons that are coordinately skipped by hnRNP C and YB-1. Although detailed functional coordination of hnRNP C and YB-1 on these targets, and involvement of hnRNP L, remain unknown, *MUSK* exon 10 is unlikely to be the only target where hnRNP C, YB-1, and hnRNP L coordinately induce exon skipping.

Recent studies of alternative splicing in different cellular and physiological states have broadened our understanding of the molecular basis for functional selection of a certain isoform in a tissue-specific and developmental stage-specific manner. These studies demonstrated multiple intriguing features of splicing regulatory factor(s) including cell-type specific expression, intracellular localization, post-translational modification on different cellular stimuli, etc. Precise regulation of cellular differentiation is indispensable for the proper development of vertebrate embryo and deregulated differentiation results in diverse human congenital abnormalities including cancers. In human myogenic cells (KD3), skipping of *MUSK* exon 10 is significantly reduced from ~41% to ~22% upon myogenic differentiation, which is in parallel with the reduced expression of hnRNP C and YB-1 (Fig. 6). We also observed a similar expression profile of *MUSK* exon 10 in primary human myoblasts (SkMC) upon myogenic differentiation (Figs. S7a, b and 6c). Reduced expression of hnRNP C, YB-1 and even hnRNP L upon myogenic differentiation is also reported in mouse myoblast cells

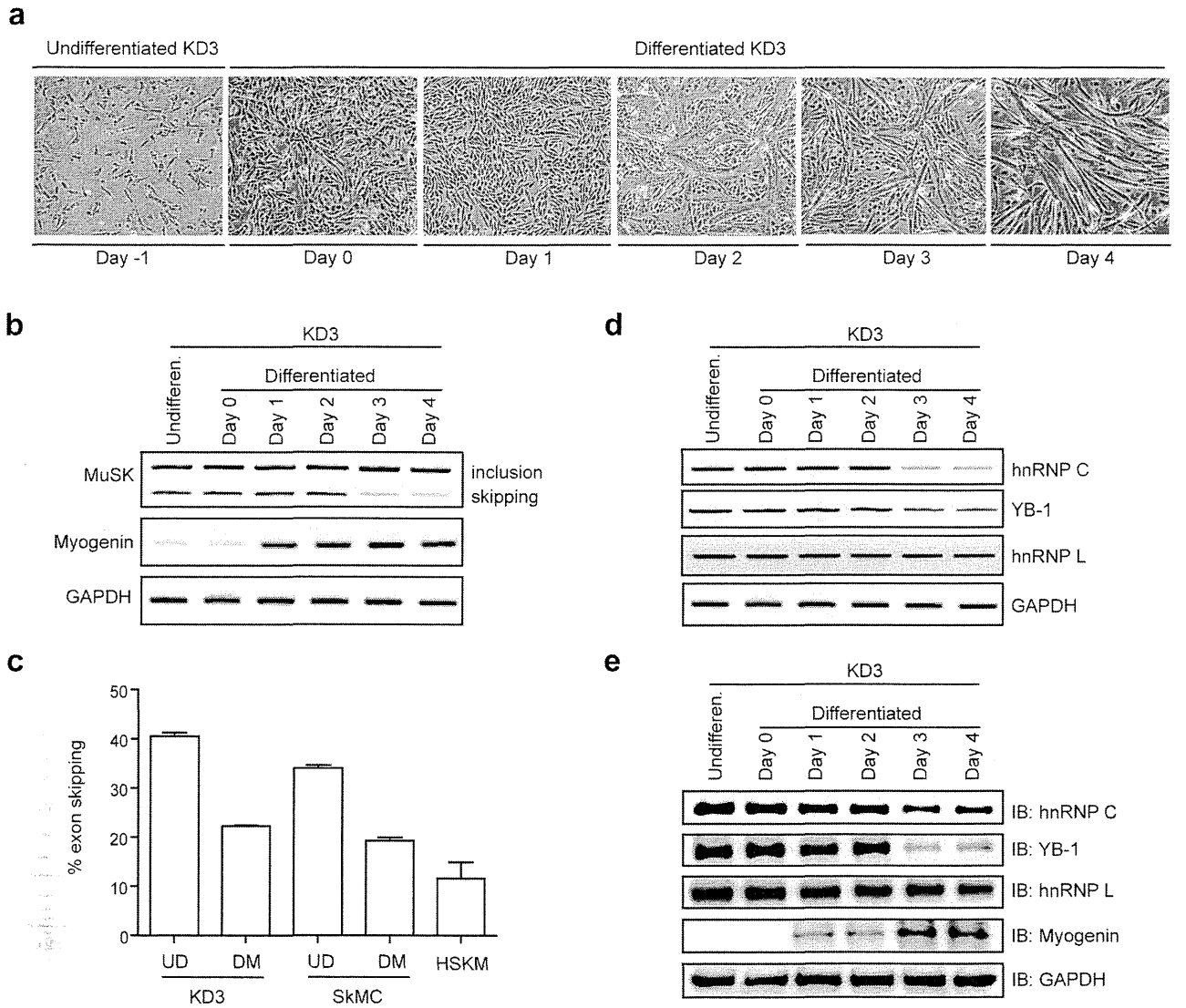

Figure 6 | Suppression of hnRNP C and YB-1 expressions in myogenic differentiation enhances inclusion of *MUSK* exon 10. (a) Phase-contrast images showing a temporal profile of differentiation of KD3 cells. (b) RT-PCR showing alternative splicing of endogenous *MUSK* exon 10 at different differentiation days of KD3 cells. (c) Real-time RT-PCR to quantify endogenous human *MUSK* transcripts. The absolute copy numbers of each isoform (Isoforms A-D, as shown in Fig. S2f) were estimated using total RNA isolated from KD3 cells, primary human myoblasts (SkMC) and human skeletal muscle (HSKM). Then the ratio of exon 10-skipping (including both isoforms C and D as shown in Fig. S2f) was determined (% exon skipping). UD, undifferentiated cells; DM, differentiated myotubes (at day 4 for KD3 and at day 8 for SkMC). Transcripts levels were normalized against GAPDH values. Bars represent mean and SD of three independent experiments. (d, e) Endogenous expression of splicing suppressors by RT-PCR (d) and immunoblotting (e) at different differentiation days of KD3 cells. Expressions of myogenin and GAPDH are shown as internal controls in panels (b), (d), and (e). The same gel image of GAPDH is used in panels (b) and (d).

(C2C12)[47,48]. Therefore, human has evolutionally acquired ESS5 to skip *MUSK* exon 10, whereas downregulation of its *trans*-factors, hnRNP C and YB-1, in muscle differentiation remains unchanged in the course of evolution. It is interesting to note that YB-1 is a negative regulator of C2C12 myoblast differentiation[48]. YB-1 cooperatively interacts with MSX1 that inhibits the expression of MyoD by binding to the core enhancer region (CER) of the MyoD promoter[48]. Therefore, reduction of YB-1 expression in the course of differentiation is physiologically relevant to facilitating myogenic differentiation.

Physiological and evolutional significance of acquisition of an exon 10-skipped Wnt-insensitive MuSK isoform in human remains elusive, although an exon 10-skipped MuSK isoform constitutes a minor fraction in human skeletal muscle. An exon 10-skipped isoform is deficient of Fz-CRD function[16,17]. In *CHRNA1* encoding AChR α subunit, only humans and great apes have acquired alternative inclusion of a non-functional exon P3A, which we have shown to be regulated by hnRNP H[41], PTB[49], and hnRNP L[38]. Although the evolutional significance of having acquired a non-functional exon P3A remains unsolved, skipping of *MUSK* exon 10 is the second defective splicing event that is unique to human. In mammals, *CHRNE* encoding the AChR ε subunit is expressed only at NMJ to promote endplate-specific expression of AChR[50-52]. Similarly, *Colq* encoding collagen Q has two promoters that are activated in slow- and fast-twitch muscles, respectively. In fast-twitch muscles, the Colq-1a promoter is activated only at NMJ[53]. Differentiation-induced inclusion of *MUSK* exon 10, as well as NMJ-specific expression of *CHRNE* and *COLQ*, suggest that human might have acquired NMJ-specific expression of a Wnt-responsive exon 10-included *MUSK* isoform to suppress extra-synaptic formation of AChR clusters. To achieve such beneficial expression, exonic splicing *cis*-elements have evolved to utilize spatiotemporally regulated expressions

of splicing *trans*-factors that were already functional in lower mammals.

Methods

Sources of human skeletal muscle RNA. To scrutinize *MUSK* isoforms in human skeletal muscle, we purchased human skeletal muscle total RNA (Clontech). We also purchased primary human skeletal muscle cells (SkMC, Lonza). Immortalized human myogenic cells (KD3) were kindly provided by Dr. Naohiro Hashimoto (National Center for Geriatrics and Gerontology, Japan)[54–56].

Cell culture and transfection. HeLa and C2C12 cells were cultured in DMEM (Sigma-Aldrich) with 10% fetal bovine serum (FBS, Sigma-Aldrich). SkMC cells were maintained in SkGM medium (Lonza). KD3 cells were grown in high-glucose (4.5 g/ml) DMEM (hDMEM) media containing 20% FCS and 2% Ultroser G serum substitute (PALL). To induce myogenic differentiation in C2C12 or SkMC, the culture medium of confluent cells was switched to DMEM supplemented with 2% horse serum. For myogenic differentiation of KD3 cells, we cultured confluent cells in hDMEM containing 5 μg/ml holo-transferrin (bovine), 10 μg/ml insulin, and 10 nM selenite (TIS, Gibco), as well as 2% FCS. HeLa and KD3 cells were transfected by FuGENE 6 (Roche) and Avalanche (EZT-HSKM-1, EZ Biosystems), respectively.

Construction of *MUSK* minigene for splicing analysis. We constructed human *MUSK* minigene spanning exons 8 to 11 in pcDNA3.1D/ V5-HiS-TOPO vector (Invitrogen) using a proofreading DNA polymerase (PrimeSTAR, Takara). Four PCR products were first amplified: exon 8 to intron 8 (IVS8+389); intron 8 (IVS8-148) to intron 9 (IVS9+121); intron 9 (IVS9-243) to intron 10 (IVS10+202); and intron 10 (IVS10-77) to exon 11. The PCR primers carried additional 5′ sequences that matched to the neighboring amplicons. Amplicons 1/2 and 3/4 were first ligated each other, respectively, and the generated fragments 1/2 and 3/4 were ligated to generate a single fragment to be cloned into pcDNA3.1D/ V5-HiS-TOPO vector. The final product, pcDNA-human-*MUSK*, thus lacked 13865, 5248, and 7426 nucleotides in the middle of introns 8, 9, and 10, respectively.

We also inserted *MUSK/Musk* exon 10 and flanking intronic sequences (245 nucleotides of intron 9 and 200 nucleotides of intron 10) of both human and mouse in the modified exon-trapping vector, pSPL3[41]. The PCR product carried NotI and PacI sites on each for cloning into pSPL3. Artificial mutations and block replacement were engineered into the pSPL3 minigenes using the QuikChange site-directed mutagenesis kit (Stratagene) (Supplementary Table 2).

We made chimeric constructs of pSPL3-human-*MUSK* carrying human and mouse segments using the megaprimer method[57]. At first, we PCR-amplified the desired mouse segment with primers that carried 20 to 25 complementary nucleotides to pSPL3-human-*MUSK* at the 5′ ends. The PCR amplicon was used as a megaprimer for the QuikChange site-directed mutagenesis kit to make chimeric pSPL3-human-*MUSK* minigenes. The entire inserts were sequenced for all the generated clones to ensure absence of PCR artifacts.

RT-PCR and real-time RT-PCR. Total RNA was extracted 40 h after transfection using Trizol (Invitrogen), followed by DNase I treatment (Qiagen). cDNA was synthesized with an oligo-dT primer (Invitrogen) using ReverTra Ace reverse transcriptase (Toyobo). RT-PCR was performed using GoTaq (Promega) (Supplementary Table 3).

Real-time RT-PCR was performed using LightCycler 480 II (Roche) and the SYBR Premix Ex Taq II (Takara) to quantify endogenous human *MUSK* transcripts. The absolute copy numbers of each of *MUSK* isoforms were estimated using specific primers (Supplementary Table 3) and cDNA fragments cloned into pGEM-T as references.

RNA-electrophoretic mobility shift assays (RNA-EMSA). ^{32}P-labeled RNA probes comprised of 20 nucleotides were transcribed *in vitro* with the T7 RiboMAX large-scale RNA production system (Promega) using ^{32}P-UTP as previously reported[58]. The template DNA for transcription was generated by overlap extension PCR using two overlapping primers (Supplementary Table 4), where T7 promoter sequence was introduced at the 5' end of the forward primer. Binding reactions were carried out using HeLa nuclear extract (CilBiotech) and radiolabeled RNA probes at 30°C for 15 min in a 15-μl reaction mixture, with a final concentration of 3.0 mM $MgCl_2$, 50 mM KCl, 20 mM Tris-HCl (pH 7.5), 0.1 mM EDTA, 0.1% (v/v) Triton X-100, 10% (v/v) glycerol, 3 μg of BSA, 1 μg of tRNA, 4 U RNasin (Promega). RNA-protein complexes were analyzed by 5% polyacrylamide gel electrophoresis (PAGE) at 4°C using 0.5× Tris-borate-EDTA (TBE) buffer. Dried gels were subjected to autoradiography.

RNA affinity purification assay. We synthesized 20-nucleotide biotinylated RNA probes with the T7 RiboMAX large-scale RNA production system (Promega) using 3.0 mM Biotin-14-CTP (Invitrogen) as described previously[38]. The template DNA was generated as described for RNA-EMSA.

The RNA affinity purification method was modified from the previously adopted protocol[38]. Biotinylated RNAs (0.75 nmol) and HeLa nuclear extract (30 μl) (CilBiotech) were mixed in a 500-μl binding buffer [20 mM HEPES, pH 7.8, 150 mM KCl, 0.1 mM EDTA, 1 mM DTT, 1 mM PMSF, 0.05% Triton X, 1× Protease Inhibitor Cocktail (Active Motif)], and were incubated at 30°C for 3 h with gentle agitation. In parallel, 50 μl streptavidin-conjugated beads (Streptavidin-sepharose, GE Healthcare) were blocked with a 1 : 1 mixture of 1 ml binding buffer containing yeast tRNA (0.1 mg/ 100 μl of beads) and 1 ml PBS containing 4% BSA at 4°C with rotation for 1 h. The beads were mixed with the binding solution for 2 h at 4°C with gentle rotation. After washing the beads four times with 1 ml binding buffer, RNA-bound proteins were eluted in SDS loading buffer by boiling at 95°C for 5 min. The isolated proteins were fractionated on a 10% SDS-polyacrylamide gel and stained with Coomassie blue or by immunoblotting.

Mass spectrometry. Mass spectrometry was performed as previously described[38].

Depletion of hnRNP C from nuclear extract. Antibody-mediated depletion of hnRNP C from HeLa cell nuclear extract was performed using Protein G HP spin trap (GE Healthcare) according to the manufacturer's instructions.

siRNA knockdown and minigene splicing. We synthesized the following human siRNAs (Sigma Genosys):

5'-CAACGGGACUAUUAUGAUATT-3' for hnRNP C;
5'-CCACGCAAUUACCAGCAAATT-3' for YB-1; and
5'-GAAUGGAGUUCAGGCGAUGTT-3' for hnRNP L.

We also synthesized a second set of human siRNAs:

5'-GUAGAGAUGAAGAAUGAUATT-3' for hnRNP C,
5'-AGAAGGUCAUCGCAACGAATT -3' for YB-1, and
5'-CUACGAUGACCCGCACAAATT-3' for hnRNP L.

The control siRNA was AllStar Negative Control siRNA (1027281) by Qiagen. Cells were plated 24 h before transfection in six-well culture plates (1.5×10^5 cells/well). The transfection reagent included each siRNA duplex at a final concentration of 30 nM, 1 μl Lipofectamine 2000 (Invitrogen), and 500 ng minigene in 100 μl Opti-MEM medium. The cells were harvested three days after transfection for RT-PCR and immunoblotting analyses.

cDNA overexpression and minigene splicing. Human hnRNP C cDNA was amplified with total RNA of human skeletal muscle (Clontech), and cloned into pCDNA3.1D/V5-His TOPO (Invitrogen) to make pcDNA-hnRNP C. We previously constructed pcDNA-hnRNP L[38]. The human YB-1 expression vector (pCMV-YB-1-myc-nuc) was kindly provided by Dr. Akira Yokomizo (Kyushu University, Japan)[59]. Cells were plated 24 h prior to transfection in a six-well culture plate (1.5×10^5 cells/well) and transfected with 1 μg of expression construct(s), 500 ng of the minigene, and 6.0 μl of FuGENE 6 (Roche) in 100 μl Opti-MEM medium. The cells were harvested three days after transfection for RT-PCR and immunoblotting analyses.

Harvesting cells for immunoblotting. Cells were washed twice in PBS and harvested in PBS with 1× Protease Inhibitor Cocktail. After centrifugation at 2,000 × *g* for 5 min, the pellets were resuspended in buffer A [10 mM HEPES-NaOH (pH 7.8), 10 mM KCl, 0.1 mM EDTA, 1 mM DTT, 0.5 mM PMSF, 0.1% Nonidet P-40, 1× Protease Inhibitor Cocktail] and kept for 30 min on ice. After sonication, samples were centrifuged at 20,000 × *g* for 5 min to remove cell debris. The total cell lysate was subjected to immunoblotting.

Tethered function assay. Tethered function assay was performed by co-transfection of a reporter minigene carrying MS2- and PP7-binding sites and effector construct(s) fused to either MS2 or PP7 coat protein. To make pcDNA-hnRNP C-MS2, an insert encoding MS2 was isolated from pcDNA-hnRNP L-MS2[38] using XhoI and XbaI restriction enzymes, purified, and cloned into the respective sites of pcDNA-hnRNP C. We purchased a vector harboring PP7 cDNA (pET22HT-PP7delFG) from Addgene. Using this vector, a PCR product spanning PP7 cDNA was amplified with primers having XhoI and XbaI sites at the 5′ ends. This was subsequently cloned into XhoI/XbaI sites of pcDNA-hnRNP L[38] to obtain pcDNA-hnRNP L-PP7. Using the In-Fusion cloning kit (Clontech), we introduced PP7 cDNA into pCMV-YB-1-myc-nuc to produce pCMV-YB-1-PP7-myc-nuc. The absence of artifacts was confirmed by sequencing the entire inserts. We previously made pcDNA-MS2 harboring only MS2 cDNA[38]. We also cloned only PP7 cDNA into pcDNA3.1D/ V5-HiS-TOPO to make pcDNA-PP7.

To construct a reporter minigene, we substituted the bacteriophage MS2 coat protein-binding hairpin RNA sequence (5'-ACATGAGGATCACCCATGT-3')[38] for the first half of the ESS5 sequence (5'-TTTTTCT-3') and PP7 coat protein-binding hairpin RNA sequence (5'-GGCACAGAAGATATGGCTTCGTGCC-3')[60] for the second half of ESS5 sequence (5'-CAACACCTC-3') in *MUSK* exon 10 in pSPL3 minigene using the QuikChange site-directed mutagenesis kit.

Antibodies. Antibodies used in this study were anti-hnRNP C1/C2 4F4 (SC-32308, Santa Cruz Biotechnology), anti-YB1 (A303-230A, Bethyl Laboratories), anti-hnRNP L 4D11 (sc-32317, Santa Cruz Biotechnology), anti-His-tag (D291-3, Medical & Biological Laboratories), anti-GAPDH (G9545, Sigma-Aldrich), anti-β-actin C4 (sc-47778, Santa Cruz Biotechnology), anti-myogenin (M-225) (sc-576, Santa Cruz Biotechnology), and anti-U2AF65 MC3 (sc-53942, Santa Cruz Biotechnology).

Co-immunoprecipitation. Protein-protein interactions were studied by the co-immunoprecipitation (Co-IP) experiment using the Nuclear Complex Co-IP kit (Active Motif) according to the manufacturer's instructions, in the presence or absence of RNase (RNase cocktail enzyme mix, Ambion). We incubated 100 μg of HeLa nuclear extract with 2 μg of anti-hnRNP C or anti-YB-1 antibody. We included isotype-matched normal IgG as a control. The binding buffer contained 150 mM

NaCl. The protein G beads with bound molecules were boiled and run on a polyacrylamide gel followed by immunoblotting.

***In silico* search for binding sites of hnRNP C and YB-1 at alternative cassette exons in the human genome.** We first searched for the hnRNP C motif ('TTTT') in human alternative cassette exons and flanking introns according to ENSEMBL 76. We then searched for the YB-1 SELEX motifs (CATC and CACC) within 5 to 16 nucleotides upstream and downstream of the hnRNP C site. We similarly identified hnRNP C-binding sites in iCLIP data[24,44]. After filtering the iCLIP sites to alternative cassette exons and flanking introns, we searched for the YB-1 SELEX motifs (CATC and CACC) within 20 nucleotides upstream and downstream of the iCLIP sites.

1. Yang, X., Li, W., Prescott, E. D., Burden, S. J. & Wang, J. C. DNA topoisomerase II beta and neural development. *Science* **287**, 131–134 (2000).
2. Yang, X. *et al.* Patterning of muscle acetylcholine receptor gene expression in the absence of motor innervation. *Neuron* **30**, 399–410 (2001).
3. Lin, W. *et al.* Distinct roles of nerve and muscle in postsynaptic differentiation of the neuromuscular synapse. *Nature* **410**, 1057–1064 (2001).
4. Arber, S., Burden, S. J. & Harris, A. J. Patterning of skeletal muscle. *Curr Opin Neurobiol* **12**, 100–103 (2002).
5. Panzer, J. A., Song, Y. & Balice-Gordon, R. J. In vivo imaging of preferential motor axon outgrowth to and synaptogenesis at prepatterned acetylcholine receptor clusters in embryonic zebrafish skeletal muscle. *J Neurosci* **26**, 934–947 (2006).
6. Kim, N. & Burden, S. J. MuSK controls where motor axons grow and form synapses. *Nat Neurosci* **11**, 19–27 (2008).
7. Kim, N. *et al.* Lrp4 is a receptor for Agrin and forms a complex with MuSK. *Cell* **135**, 334–342 (2008).
8. Zhang, B. *et al.* LRP4 serves as a coreceptor of agrin. *Neuron* **60**, 285–297 (2008).
9. Zhang, W., Coldefy, A. S., Hubbard, S. R. & Burden, S. J. Agrin binds to the N-terminal region of Lrp4 protein and stimulates association between Lrp4 and the first immunoglobulin-like domain in muscle-specific kinase (MuSK). *J Biol Chem* **286**, 40624–40630 (2011).
10. Masiakowski, P. & Yancopoulos, G. D. The Wnt receptor CRD domain is also found in MuSK and related orphan receptor tyrosine kinases. *Curr Biol* **8**, R407–R407 (1998).
11. Xu, Y. K. & Nusse, R. The Frizzled CRD domain is conserved in diverse proteins including several receptor tyrosine kinases. *Curr Biol* **8**, R405–R406 (1998).
12. Stiegler, A. L., Burden, S. J. & Hubbard, S. R. Crystal structure of the frizzled-like cysteine-rich domain of the receptor tyrosine kinase MuSK. *J Mol Biol* **393**, 1–9 (2009).
13. Roszmusz, E., Patthy, A., Trexler, M. & Patthy, L. Localization of disulfide bonds in the frizzled module of Ror1 receptor tyrosine kinase. *J Biol Chem* **276**, 18485–18490 (2001).
14. Jennings, C. G., Dyer, S. M. & Burden, S. J. Muscle-specific trk-related receptor with a kringle domain defines a distinct class of receptor tyrosine kinases. *Proc Natl Acad Sci U S A* **90**, 2895–2899 (1993).
15. Valenzuela, D. M. *et al.* Receptor Tyrosine Kinase Specific for the Skeletal-Muscle Lineage - Expression in Embryonic Muscle, at the Neuromuscular-Junction, and after Injury. *Neuron* **15**, 573–584 (1995).
16. Zhang, B. *et al.* Wnt proteins regulate acetylcholine receptor clustering in muscle cells. *Mol Brain* **5**, 7 (2012).
17. Strochlic, L. *et al.* Wnt4 participates in the formation of vertebrate neuromuscular junction. *PLoS One* **7**, e29976 (2012).
18. Jing, L., Lefebvre, J. L., Gordon, L. R. & Granato, M. Wnt signals organize synaptic prepattern and axon guidance through the zebrafish unplugged/MuSK receptor. *Neuron* **61**, 721–733 (2009).
19. Gordon, L. R., Gribble, K. D., Syrett, C. M. & Granato, M. Initiation of synapse formation by Wnt-induced MuSK endocytosis. *Development* **139**, 1023–1033 (2012).
20. Jing, L., Gordon, L. R., Shtibin, E. & Granato, M. Temporal and spatial requirements of unplugged/MuSK function during zebrafish neuromuscular development. *PLoS One* **5**, e8843 (2010).
21. Zhang, J., Lefebvre, J. L., Zhao, S. & Granato, M. Zebrafish unplugged reveals a role for muscle-specific kinase homologs in axonal pathway choice. *Nat Neurosci* **7**, 1303–1309 (2004).
22. Zhou, H., Glass, D. J., Yancopoulos, G. D. & Sanes, J. R. Distinct domains of MuSK mediate its abilities to induce and to associate with postsynaptic specializations. *J Cell Biol* **146**, 1133–1146 (1999).
23. Antolik, C., Catino, D. H., Resneck, W. G. & Bloch, R. J. The tetratricopeptide repeat domains of rapsyn bind directly to cytoplasmic sequences of the muscle-specific kinase. *Neuroscience* **141**, 87–100 (2006).
24. Zarnack, K. *et al.* Direct competition between hnRNP C and U2AF65 protects the transcriptome from the exonization of Alu elements. *Cell* **152**, 453–466 (2013).
25. Shetty, S. Regulation of urokinase receptor mRNA stability by hnRNP C in lung epithelial cells. *Mol Cell Biochem* **272**, 107–118 (2005).
26. Lee, E. K. *et al.* hnRNP C promotes APP translation by competing with FMRP for APP mRNA recruitment to P bodies. *Nat Struct Mol Biol* **17**, 732–739 (2010).
27. McCloskey, A., Taniguchi, I., Shinmyozu, K. & Ohno, M. hnRNP C tetramer measures RNA length to classify RNA polymerase II transcripts for export. *Science* **335**, 1643–1646 (2012).
28. Kohno, K., Izumi, H., Uchiumi, T., Ashizuka, M. & Kuwano, M. The pleiotropic functions of the Y-box-binding protein, YB-1. *Bioessays* **25**, 691–698 (2003).
29. Wei, W. J. *et al.* YB-1 binds to CAUC motifs and stimulates exon inclusion by enhancing the recruitment of U2AF to weak polypyrimidine tracts. *Nucleic Acids Res* **40**, 8622–8636 (2012).
30. Hung, L. H. *et al.* Diverse roles of hnRNP L in mammalian mRNA processing: a combined microarray and RNAi analysis. *RNA* **14**, 284–296 (2008).
31. Rossbach, O. *et al.* Crosslinking-immunoprecipitation (iCLIP) analysis reveals global regulatory roles of hnRNP L. *RNA Biol* **11**, 146–155 (2014).
32. Hui, J. *et al.* Intronic CA-repeat and CA-rich elements: a new class of regulators of mammalian alternative splicing. *EMBO J* **24**, 1988–1998 (2005).
33. Hui, J., Stangl, K., Lane, W. S. & Bindereif, A. HnRNP L stimulates splicing of the eNOS gene by binding to variable-length CA repeats. *Nat Struct Biol* **10**, 33–37 (2003).
34. Chiou, N. T., Shankarling, G. & Lynch, K. W. hnRNP L and hnRNP A1 induce extended U1 snRNA interactions with an exon to repress spliceosome assembly. *Mol Cell* **49**, 972–982 (2013).
35. House, A. E. & Lynch, K. W. An exonic splicing silencer represses spliceosome assembly after ATP-dependent exon recognition. *Nat Struct Mol Biol* **13**, 937–944 (2006).
36. Motta-Mena, L. B., Heyd, F. & Lynch, K. W. Context-dependent regulatory mechanism of the splicing factor hnRNP L. *Mol Cell* **37**, 223–234 (2010).
37. Tong, A., Nguyen, J. & Lynch, K. W. Differential expression of CD45 isoforms is controlled by the combined activity of basal and inducible splicing-regulatory elements in each of the variable exons. *J Biol Chem* **280**, 38297–38304 (2005).
38. Rahman, M. A. *et al.* HnRNP L and hnRNP LL antagonistically modulate PTB-mediated splicing suppression of CHRNA1 pre-mRNA. *Sci Rep* **3**, 2931 (2013).
39. Guang, S., Felthauser, A. M. & Mertz, J. E. Binding of hnRNP L to the pre-mRNA processing enhancer of the herpes simplex virus thymidine kinase gene enhances both polyadenylation and nucleocytoplasmic export of intronless mRNAs. *Mol Cell Biol* **25**, 6303–6313 (2005).
40. Hui, J., Reither, G. & Bindereif, A. Novel functional role of CA repeats and hnRNP L in RNA stability. *RNA* **9**, 931–936 (2003).
41. Masuda, A. *et al.* hnRNP H enhances skipping of a nonfunctional exon P3A in CHRNA1 and a mutation disrupting its binding causes congenital myasthenic syndrome. *Hum Mol Genet* **17**, 4022–4035 (2008).
42. Schaal, T. D. & Maniatis, T. Multiple distinct splicing enhancers in the protein-coding sequences of a constitutively spliced pre-mRNA. *Mol Cell Biol* **19**, 261–273 (1999).
43. Black, D. L. Mechanisms of alternative pre-messenger RNA splicing. *Annu Rev Biochem* **72**, 291–336 (2003).
44. Konig, J. *et al.* iCLIP reveals the function of hnRNP particles in splicing at individual nucleotide resolution. *Nat Struct Mol Biol* **17**, 909–915 (2010).
45. Wang, Y. *et al.* A complex network of factors with overlapping affinities represses splicing through intronic elements. *Nat Struct Mol Biol* **20**, 36–45 (2013).
46. Rideau, A. P. *et al.* A peptide motif in Raver1 mediates splicing repression by interaction with the PTB RRM2 domain. *Nat Struct Mol Biol* **13**, 839–848 (2006).
47. Bland, C. S. *et al.* Global regulation of alternative splicing during myogenic differentiation. *Nucleic Acids Res* **38**, 7651–7664 (2010).
48. Song, Y. J. & Lee, H. YB1/p32, a nuclear Y-box binding protein 1, is a novel regulator of myoblast differentiation that interacts with Msx1 homeoprotein. *Exp Cell Res* **316**, 517–529 (2010).
49. Bian, Y. *et al.* Tannic acid facilitates expression of the polypyrimidine tract binding protein and alleviates deleterious inclusion of CHRNA1 exon P3A due to an hnRNP H-disrupting mutation in congenital myasthenic syndrome. *Hum Mol Genet* **18**, 1229–1237 (2009).
50. Koike, S., Schaeffer, L. & Changeux, J. P. Identification of a DNA element determining synaptic expression of the mouse acetylcholine receptor delta-subunit gene. *Proc Natl Acad Sci U S A* **92**, 10624–10628 (1995).
51. Duclert, A., Savatier, N., Schaeffer, L. & Changeux, J. P. Identification of an element crucial for the sub-synaptic expression of the acetylcholine receptor epsilon-subunit gene. *J Biol Chem* **271**, 17433–17438 (1996).
52. Ohno, K., Anlar, B. & Engel, A. G. Congenital myasthenic syndrome caused by a mutation in the Ets-binding site of the promoter region of the acetylcholine receptor epsilon subunit gene. *Neuromuscul Disord* **9**, 131–135 (1999).
53. Lee, H. H. *et al.* Transcriptional regulation of acetylcholinesterase-associated collagen ColQ: differential expression in fast and slow twitch muscle fibers is driven by distinct promoters. *J Biol Chem* **279**, 27098–27107 (2004).
54. Shiomi, K. *et al.* CDK4 and cyclin D1 allow human myogenic cells to recapture growth property without compromising differentiation potential. *Gene Ther* **18**, 857–866 (2011).
55. Wada, M. R., Inagawa-Ogashiwa, M., Shimizu, S., Yasumoto, S. & Hashimoto, N. Generation of different fates from multipotent muscle stem cells. *Development* **129**, 2987–2995 (2002).
56. Hashimoto, N. *et al.* Immortalization of human myogenic progenitor cell clone retaining multipotentiality. *Biochem Biophys Res Commun* **348**, 1383–1388 (2006).

57. Ohno, K. *et al.* Myasthenic syndromes in Turkish kinships due to mutations in the acetylcholine receptor. *Ann Neurol* **44**, 234–241 (1998).
58. Mayeda, A. & Krainer, A. R. Mammalian in vitro splicing assays. *Methods Mol Biol* **118**, 315–321 (1999).
59. Shiota, M. *et al.* Y-box binding protein-1 promotes castration-resistant prostate cancer growth via androgen receptor expression. *Endocr Relat Cancer* **18**, 505–517 (2011).
60. Chao, J. A., Patskovsky, Y., Almo, S. C. & Singer, R. H. Structural basis for the coevolution of a viral RNA-protein complex. *Nat Struct Mol Biol* **15**, 103–105 (2008).

Acknowledgments

We are grateful to Dr. Akira Yokomizo (Kyushu University, Japan) for providing pCMV-YB-1-myc-nuc expression vector, to Dr. Naohiro Hashimoto (National Center for Geriatrics and Gerontology, Japan) for providing KD3 cells, and to Dr. Kentaro Taki (Nagoya University) for technical assistance on the mass spectrometry analysis. This work was supported by Grants-in-Aid from the MEXT and MHLW of Japan.

Author contributions

Ki.O. conceived the project. F.N., M.A.R. and A.M. designed experiments; F.N. performed most of the experiments; M.A.R. contributed to RNA affinity purification assay and mass spectrometry analysis; Ke.O. and J.T. contributed to RNA-EMSA and *in silico* analysis, respectively. F.N., M.A.R. and Ki.O. wrote the paper.

Additional information

Supplementary information accompanies this paper at http://www.nature.com/scientificreports

Competing financial interests: The authors declare no competing financial interests.

How to cite this article: Nasrin, F. *et al.* HnRNP C, YB-1 and hnRNP L coordinately enhance skipping of human *MUSK* exon 10 to generate a Wnt-insensitive MuSK isoform. *Sci. Rep.* **4**, 6841; DOI:10.1038/srep06841 (2014).

Available online at www.sciencedirect.com

ScienceDirect

Neuromuscular Disorders ■■ (2014) ■■–■■

www.elsevier.com/locate/nmd

Congenital myasthenic syndrome in Japan: Ethnically unique mutations in muscle nicotinic acetylcholine receptor subunits

Yoshiteru Azuma [a,b], Tomohiko Nakata [a,b], Motoki Tanaka [c], Xin-Ming Shen [d], Mikako Ito [a], Satoshi Iwata [a], Tatsuya Okuno [a], Yoshiko Nomura [e], Naoki Ando [f], Keiko Ishigaki [g], Bisei Ohkawara [a], Akio Masuda [a], Jun Natsume [b], Seiji Kojima [b], Masahiro Sokabe [c], Kinji Ohno [a,*]

[a] *Division of Neurogenetics, Center for Neurological Diseases and Cancer, Nagoya University Graduate School of Medicine, Nagoya, Japan*
[b] *Department of Pediatrics, Nagoya University Graduate School of Medicine, Nagoya, Japan*
[c] *Department of Physiology, Nagoya University Graduate School of Medicine, Nagoya, Japan*
[d] *Department of Neurology, Mayo Clinic, Rochester, MN, USA*
[e] *Segawa Neurological Clinic for Children, Tokyo, Japan*
[f] *Department of Pediatrics, Nagoya City University Graduate School of Medicine, Nagoya, Japan*
[g] *Department of Pediatrics, Tokyo Women's Medical University, Tokyo, Japan*

Received 29 May 2014; received in revised form 9 August 2014; accepted 3 September 2014

Abstract

Congenital myasthenic syndromes (CMS) are caused by mutations in genes expressed at the neuromuscular junction. Most CMS patients have been reported in Western and Middle Eastern countries, and only four patients with *COLQ* mutations have been reported in Japan. We here report six mutations in acetylcholine receptor (AChR) subunit genes in five Japanese patients. Five mutations are novel, and one mutation is shared with a European American patient but with a different haplotype. Among the observed mutations, p.Thr284Pro (p.Thr264Pro according to the legacy annotation) in the epsilon subunit causes a slow-channel CMS. Five other mutations in the delta and epsilon subunits are splice site, frameshift, null, or missense mutations causing endplate AChR deficiency. We also found a heteroallelic p.Met465Thr in the beta subunit in another patient. p.Met465Thr, however, was likely to be polymorphism, because single channel recordings showed mild shortening of channel openings without affecting cell surface expression of AChR, and the minor allelic frequency of p.Met465Thr was 5.1% in the Japanese population. Lack of shared mutant alleles between the Japanese and the other patients suggests that most mutations described here are ethnically unique or *de novo* in each family.

Keywords: Congenital myasthenic syndromes; Acetylcholine receptor; Slow channel syndrome; Fast channel syndrome; Endplate acetylcholine receptor deficiency

1. Introduction

Acetylcholine released from the nerve terminal binds to muscle nicotinic acetylcholine receptor (AChR) at the motor endplate. AChR is clustered at the neuromuscular junction (NMJ) by binding to rapsyn with a stoichiometry of rapsyn to AChR of 1:1 to 2:1 [1]. AChR clustering is mediated by neural agrin that is released from the nerve terminal [2]. In early embryonic development, AChR clustering is also mediated by Wnt ligands [3,4]. Embryonic AChR is composed of α, β, δ, and γ subunits with a stoichiometry of $\alpha_2\beta\delta\gamma$. After birth, the ε subunit is substituted for the γ subunit, generating $\alpha_2\beta\delta\varepsilon$-AChR.

Congenital myasthenic syndromes (CMS) are heterogeneous disorders caused by mutations in genes expressed at the NMJ [5]. They are characterized by fatigable muscle weakness, variable muscle atrophy, and sometimes dysmorphic features. CMS mutations have been reported in 19 genes, with most mutations in *CHRNA1*, *CHRNB1*, *CHNRD*, and *CHNRE* encoding the AChR α, β, δ, and ε subunits, respectively. These mutations fall into three subsets: i) slow-channel CMS (SCCMS), in which the open time of AChR is abnormally prolonged; ii) fast-channel CMS (FCCMS), in which the open time of AChR is abnormally brief; and iii) endplate AChR deficiency. SCCMS is caused by a gain-of-function mutation and is dominantly inherited with variable penetrance [6]. In contrast, FCCMS and endplate AChR deficiency are caused by loss-of-function mutations on both alleles, and are recessively

* Corresponding author. Division of Neurogenetics, Center for Neurological Disease and Cancer, Nagoya University Graduate School of Medicine, 65 Tsurumai, Showa-ku, Nagoya 466-8550, Japan. Tel.: +81 52 744 2446; fax: +81 52 744 2449.
E-mail address: ohnok@med.nagoya-u.ac.jp (K. Ohno).

http://dx.doi.org/10.1016/j.nmd.2014.09.002

Please cite this article in press as: Yoshiteru Azuma, et al., Congenital myasthenic syndrome in Japan: Ethnically unique mutations in muscle nicotinic acetylcholine receptor subunits, Neuromuscular Disorders (2014), doi: 10.1016/j.nmd.2014.09.002

inherited. Low-expressor mutations of the AChR ε subunit are partly compensated for by expression of the embryonic AChR γ subunit, whereas the other AChR subunits have no substituting subunits. Accordingly, null and frameshift mutations are frequently detected in *CHRNE*, but not in the other subunit genes.

More than 500 patients with CMS have been reported in Western and Middle Eastern countries, whereas only four Japanese CMS patients carrying five mutations in *COLQ* encoding collagen Q that anchors acetylcholinesterase (AChE) at the NMJ have been reported by us [7,8]. Among the more than 450 CMS mutations in 19 disease genes registered in the Human Gene Mutation Database (http://www.hgmd.org), two likely have founder effects: p.Asn88Lys in *RAPSN* [9–11] and c.1124_1127dupTGCC in *DOK7* [12], whereas the others are private mutations occurring in a single or a small number of unrelated families. We here report five Japanese CMS patients with six mutations in the AChR subunit genes. We show that all the ten mutations in *COLQ*, *CHRND*, and *CHRNE* in Japanese patients are ethnically unique, which indicates that most CMS mutations arose *de novo* in recent human history or in each family.

2. Materials and methods

2.1. Ethical approval

All the human studies were approved by the institutional review boards of Nagoya University Graduate School of Medicine, Mayo Clinic, Segawa Neurological Clinic for Children, Nagoya City University, and Tokyo Women's Medical University. Appropriate written informed consent was obtained from all the patients and family members.

2.2. Mutation analysis and splicing analysis

Genomic DNA was isolated from peripheral blood with QIAamp Blood Kit (QIAGEN). We directly sequenced all exons with their flanking noncoding regions of *CHRNE*, *CHRNA1*, *CHRNB1*, and *CHRND* in this order with CEQ 8000 (Beckman Coulter). To look for large-scale DNA rearrangements in patient (Pt.) 4, we performed mate-pair sequencing of the whole genome using SOLiD4 (Life Technologies). The mate-pair library was made to span ~2 kb genomic segments according to the manufacturer's protocols. A total of 14.9 Gb of reads were mapped to human genome GRCh37/hg19 with the mapping efficiency of 89% using CLC Genomics Workbench (CLC Bio). All the reads mapped to *CHRNE* were visually scrutinized using Integrative Genome Browser (Broad Institute). Total RNA was isolated from biopsied muscle that was obtained for histopathological diagnostic purposes using RNeasy mini kit (QIAGEN). cDNA was synthesized with ReverTra Ace (Toyobo) and Oligo(dT) Primer (Life Technologies).

2.3. Expression of AChR subunit genes in HEK293 cells

Human α, β, δ, and ε subunit cDNAs were cloned into the CMV-based vector pRBG4 for expression in HEK293 cells [13]. The identified mutations were engineered into wild-type AChR subunit cDNAs in pRBG4 using the QuikChange site-directed mutagenesis kit (Stratagene). Presence of each mutation and absence of unwanted artifacts were confirmed by sequencing the entire inserts. HEK293 cells were transfected with pRBG4-α, -β, -δ, -ε, and pcDNA3.1-EGFP at a ratio of 2:1:1:1:1 using FuGENE 6 transfection reagent (Promega). After 48 hrs, cells were incubated with α-bungarotoxin Alexa Flour 647 (Life Technologies) (1:200) in PBS for 1 hr. Signals were observed under an Olympus BX60 fluorescence microscope. The cells were trypsinized, washed with PBS, and resuspended in PBS. The total number of α-bungarotoxin-binding sites on the cell surface and EGFP was determined by the FACSCalibur system (BD Biosciences).

2.4. Single channel recordings

HEK293 cells were transfected with pRBG4-α, -β, -δ, and -ε, and pEGFP-N1 at a ratio of 2:1:1:1:1, using FuGENE 6. Recordings were obtained at 24 hrs after transfection in the cell-attached configuration at a membrane potential of –80 mV at 22 °C and with bath and pipette solutions containing (in mM): KCl, 142; NaCl, 5.4; CaCl2, 1.8; MgCl2, 1.7; HEPES, 10, pH 7.4. Single-channel currents were recorded using an Axopatch 200B amplifier (Axon Instruments) at a bandwidth of 50 kHz, digitized at 5-μs intervals using Digidata 1322A (Axon Instruments) and recorded to a hard disk using the program Clampex 8.2 (Axon Instruments). Recordings obtained with ACh at 1 μM or less were analyzed at a uniform bandwidth of 10–11.7 kHz with dead time of 15.3–17.9 μs imposed. Recordings obtained with ACh at 10 μM or more were analyzed with dead time at 25 μs at 10 kHz with TAC software (Ver. x4.0.9, Bruxton). Dwell-time histograms were plotted on a logarithmic abscissa and fitted by the sum of exponentials by maximum likelihood, as previously reported [14].

3. Results

3.1. Clinical features

All Pts. had an abnormal decremental response to repetitive nerve stimulation, and no anti-AChR and anti-MuSK antibodies. Clinical features and repetitive nerve stimulation results are summarized in Table 1.

Pt. 1 (13 y.o., male) had eyelid ptosis since age six months and a positive edrophonium test. Clinical features were previously reported in a local journal [15]. Steroid pulse therapy at ages four and five years and thymectomy at age six years had no effect. Combined use of distigmine 3 mg/day and pyridostigmine 180 mg/day enabled him to sit in a chair without assistance at age 13 years. Biopsy of deltoid muscle at age eleven years showed marked AChR deficiency by fluorescent staining with α-bungarotoxin and simplified endplates by electron microscopy.

Pt. 2 (26 y.o., female) had nasal obstruction since birth and eyelid ptosis since age one month. She had a positive edrophonium test and was thought to have myasthenia gravis. Cholinesterase inhibitors were mildly effective. She has ophthamoparesis, and is able to walk but is unable to run.

Please cite this article in press as: Yoshiteru Azuma, et al., Congenital myasthenic syndrome in Japan: Ethnically unique mutations in muscle nicotinic acetylcholine receptor subunits, Neuromuscular Disorders (2014), doi: 10.1016/j.nmd.2014.09.002

Table 1
Clinical features of six patients.

Pt.	Sex	Age	Onset	Consanguinity	Repetitive N. stimulation[a]	Drug[b]
1	M	13 y	6 m	–	Accessory N., 60%; Ulnar N., 53%	Distigmine 3 mg + pyridostigmine 180 mg, effective; 3,4-DAP 40 mg, mildly effective
2	F	26 y	1 m	+	Ulnar N., 80%	Pyridostigmine 150–180 mg, mildly effective
3	F	38 y	1 y	–	Ulnar N., 81%	Pyridostigmine 90–160 mg, moderately effective
4	F	6 y	2 y	–	Median N., 60%; Ulnar N., 68%	Pyridostigmine 90 mg + 3,4-DAP 30 mg, mildly effective; ephedrine 25 mg, effective
5	M	26 y	1 m	+	Ulnar N., 76%	Pyridostigmine 135 mg, moderately effective
6	M	11 y	Birth	–	Median N., 35%; Ulnar N., 31%	Prednisolone 35 mg *dieb. alt.*, effective

[a] Repetitive N. stimulation, repetitive nerve stimulation at 2–3 Hz. Relative amplitudes of the 5th CMAP are indicated. [b] Simultaneous prescription is indicated by "+".

Pt. 3 (38 y.o., female) had ptosis at age one year and was diagnosed to have myasthenia gravis at age seven years. Since then, she has been taking cholinesterase inhibitors and prednisolone, which seemed to help but could not climb steps after age 19 years.

Pt. 4 (6 y.o., female) walked alone at age 18 months, but since age two years she had repeated episodes of generalized muscle weakness that lasted about a week, especially when having a common cold. She could walk alone but was positive for a Gowers' sign. Cholinesterase inhibitors were moderately effective. Neurological examination of the mother detected no abnormality. The father was asymptomatic according to the mother, but was not examined by us. Clinical features were previously reported as patient 4 in a local journal [16].

Pt. 5 (26 y.o., male) had feeding difficulty at age one month and had eyelid ptosis since age five months. He has weak facial muscles and is unable to run. At age seven years, he had generalized muscle weakness during an upper respiratory infection. The edrophonium test was positive.

Pt. 6 (11 y.o., male) had repeated respiratory distress and respiratory infection during infancy. He walked alone at age one year, but was noticed to walk slowly at age five years with frequent falling episodes. Rest for a short time improved his walking, but there was no diurnal fluctuation of the symptoms. Intravenous administration of edrophonium chloride ameliorated walking difficulty, but long-acting cholinesterase inhibitors had no effect.

3.2. Mutation analysis

We directly sequenced AChR subunit genes in Pts. 1–6, and identified six mutations in *CHRND* and *CHRNE*, as well as a polymorphism in *CHRNB1* (Table 2). In this study, approved nucleotide and amino acid positions are used instead of the legacy annotation, in which nucleotide and amino acid positions start from the initiation sites of mature peptides.

Pt. 1 was compound heterozygous for c.1372-1G>A at the 3′ end of intron 11 of *CHRND* and c.127C>T predicting p.Arg44Trp at the extracellular domain of the δ subunit (Fig. 1A). cDNA extracted from biopsied muscle revealed that a newly generated 'ag' dinucleotide that was one nucleotide downstream of the native 'ag' was used as a splice acceptor site (Fig. 1B), which predicted p.Glu458Argfs*20 in the long cytoplasmic loop of the δ subunit (Fig. 1A). Pt. 2 was homozygous for c.655_665del predicting p.Gly219Argfs*7 in the extracellular domain of the ε subunit (Fig. 1A). Pt. 3 was heterozygous for p.Tyr262Ter in the M1 transmembrane domain of the ε subunit (Fig. 1A). Pt. 4 was heterozygous for p.Thr284Pro in the M2 transmembrane domain of the ε subunit (Fig. 1A). Pt. 5 was homozygous for p.Leu304Arg in the short extracellular link between the M2 and M3 transmembrane domains of the ε subunit (Fig. 1A). Pt. 6 was heterozygous for p.Met465Thr close to the C-terminal end of the long cytoplasmic loop connecting the M3 and M4 transmembrane domains of AChR β subunit (Fig. 1A).

Table 2
Six mutations and one polymorphism identified in AChR subunit genes.

Pt.	Gene	Nucleotide change[c]	Amino-acid change[c]	Legacy annotation[d]	Phenotypic consequence
1	*CHRND*	c.1372-1G>A	δp.Glu458Argfs*20	δE437fs	AChR deficiency
	CHRND	c.127C>T	δp.Arg44Trp	δR23W	AChR deficiency
2[a]	*CHRNE*	c.655_665del	εp.Gly219Argfs*7	εG199fs	AChR deficiency
3[b]	*CHRNE*	c.786C>G	εp.Tyr262Ter	εY242X	AChR deficiency
4	*CHRNE*	c.850A>C	εp.Thr284Pro	εT264P	SCCMS
5[a]	*CHRNE*	c.911T>G	εp.Leu304Arg	εL284R	AChR deficiency
6	*CHRNB1*	c.1394T>C	εp.Met465Thr	βM442T	~50% shortening of AChR openings

[a] Patient is homozygous for the mutation.
[b] A mutation on another allele remains unidentified.
[c] Nucleotide and amino acid positions start from the translational start sites.
[d] In legacy annotation, nucleotide and amino acid positions start from the initiation sites of mature peptides, which are 69 nt. (23 amino acids), 63 nt. (21 amino acids), and 60 nt. (20 amino acids) downstream of the translational start sites of *CHRNB1*, *CHRND*, and *CHRNE*, respectively.

Please cite this article in press as: Yoshiteru Azuma, et al., Congenital myasthenic syndrome in Japan: Ethnically unique mutations in muscle nicotinic acetylcholine receptor subunits, Neuromuscular Disorders (2014), doi: 10.1016/j.nmd.2014.09.002

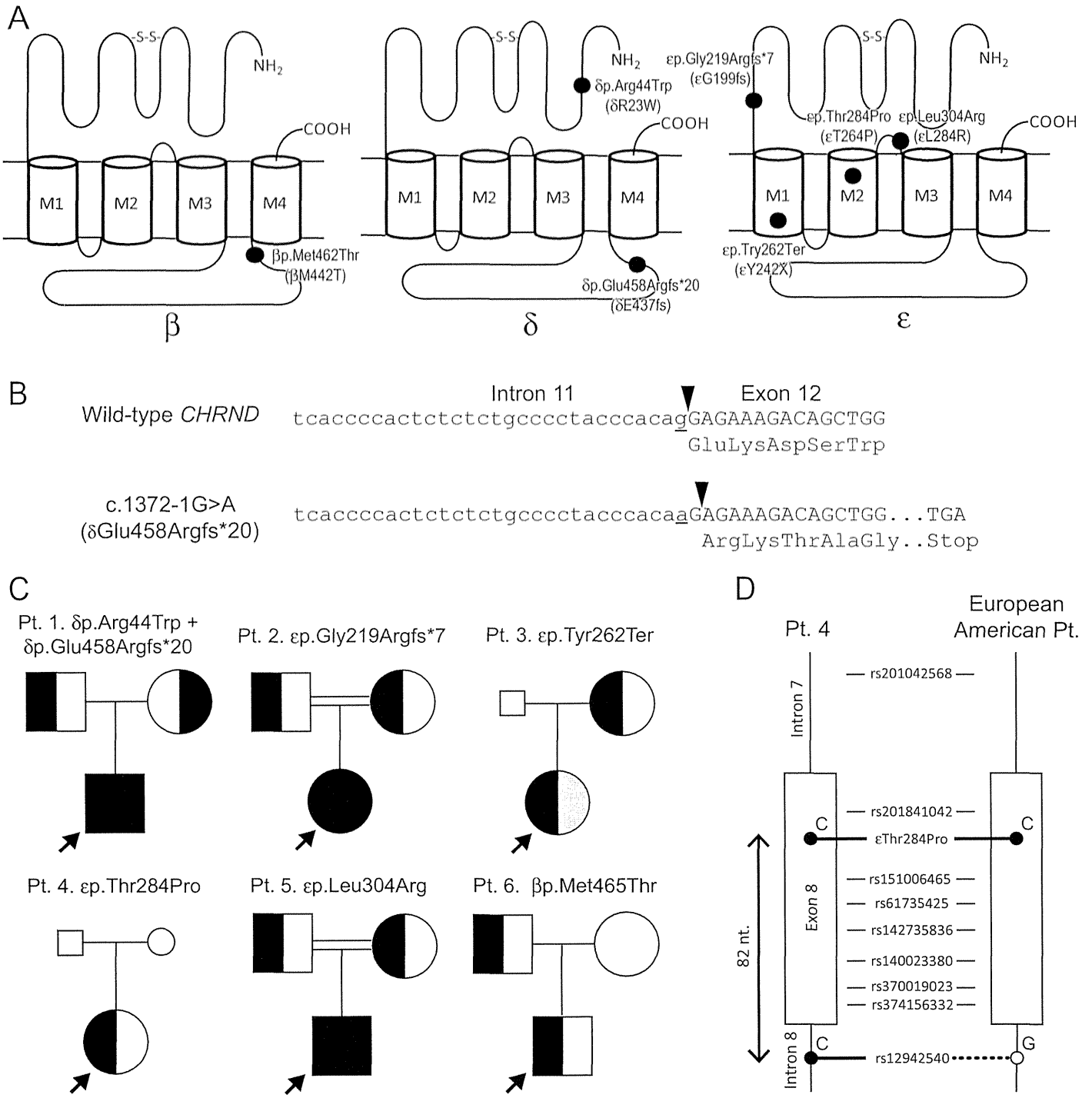

Fig. 1. Six mutations and a single polymorphism in AChR subunit genes identified in six CMS patients. (A) Positions of six mutations and a polymorphism. M1-M4, the first to fourth transmembrane domains. The M2 domains form a channel pore of AChR. (B) RT-PCR of biopsied muscle of Pt. 1 reveals that c.1372-1G>A (underlined) shifts a splice acceptor site (arrowheads) one nucleotide downstream, which predicts a shift in the reading frame (δp.Glu458Argfs*20). (C) Pedigree analyses of the mutations. Patients are indicated by arrows. Full and half shaded symbols represent homozygous and heterozygous mutations, respectively. Gray half shaded symbols represent that the individuals are predicted to carry a heterozygous mutation, the identity of which, however, has not been identified. Small symbols indicate that DNA is not available. (D) Haplotype analysis of εp.Thr284Pro in Pt. 4 and the previously reported European American Pt [7]. Both patients carry discordant nucleotides at rs12942540, which is 82 nt. downstream of the mutation.

δp.Arg44Trp (rs55868108) in Pt. 1 was previously reported in one of five healthy controls, but its ethnic origin was not documented [17]. δp.Arg44Trp, however, is not observed in the 1000 genome project (http://www.1000genomes.org/) or in the human gene variation database (HGVD), which collates SNPs in a large cohort of Japanese individuals (http://www.genome.med.kyoto-u.ac.jp/SnpDB/) [18]. As indicated below, functional analysis disclosed that δp.Arg44Trp

Please cite this article in press as: Yoshiteru Azuma, et al., Congenital myasthenic syndrome in Japan: Ethnically unique mutations in muscle nicotinic acetylcholine receptor subunits, Neuromuscular Disorders (2014), doi: 10.1016/j.nmd.2014.09.002

Table 3
Open intervals and bursts of wild-type and mutant AChR expressed on HEK cells.

	Open intervals		Bursts	
	Wild-type	βp.Met465Thr	Wild-type	βp.Met465Thr
τ_1 (ms)	0.037 ± 0.0033[a]	0.022[b]	0.036 ± 0.0017[c]	0.039 ± 0.006[d]
(a_1)	(0.17 ± 0.022)	(0.18)	(0.24 ± 0.021)	(0.18 ± 0.034)
τ_2 (ms)	0.31 ± 0.050	0.16 ± 0.017[e]	0.47 ± 0.059	0.16 ± 0.037[f]
(a_2)	(0.27 ± 0.038)	(0.23 ± 0.031)	(0.21 ± 0.027)	(0.23 ± 0.010)
τ_3 (ms)	1.35 ± 0.051	0.98 ± 0.034	3.31 ± 0.12	1.93 ± 0.085
(a_3)	(0.67 ± 0.042)	(0.78 ± 0.028)	(0.58 ± 0.038)	(0.82 ± 0.034)

Twenty-one wild-type and seven mutant patches were analyzed. Time constants, τ_n, and fractional areas, a_n, for each component are presented with mean ± SEM. ACh concentration was 50–100 nM.
[a–f] Not detected at 12, 6, 3, 5, 1, and 3 patches, respectively.
Final band widths were 11.7 and 10 kHz for wild-type and mutant AChRs, respectively.

significantly reduces cell surface expression of AChR and is unlikely to be polymorphism.

p.Met465Thr (rs201776800) in Pt. 6 was observed in eight alleles in eight Japanese individuals in the 1000 genome project with a minor allelic frequency (MAF) of 0.004, as well as in 119 alleles in a cohort of 1170 Japanese individuals in HGVD with a MAF of 0.051. Although p.Met465Thr was likely to be a polymorphism according to the high MAFs in the Japanese, we scrutinized functional consequences of p.Met465Thr in this study.

*3.3. εp.Gly219Argfs*7, εp.Tyr262Ter, and δp.Glu458Argfs*20 are predicted to compromise AChR expression*

Among the six mutations, εp.Gly219Argfs*7 in Pt. 2 and εp.Tyr262Ter in Pt. 3 were predicted to produce truncated ε subunits. We previously reported that truncation mutations in the εsubunit lead to expression of the embryonic $\alpha_2\beta\delta\gamma$-AChR at the patient's endplates and the patients have endplate AChR deficiency [19–21]. The ε mutations in Pts. 2 and 3 were thus predicted to cause AChR deficiency.

δp.Glu458Argfs*20 in Pt. 1 was predicted to generate a truncated δ subunit that cannot be incorporated into mature AChR. The phenotype of Pt. 1 is thus determined by δp.Arg44Trp on the other allele, which causes AChR deficiency as indicated below.

3.4. εp.Thr284Pro is an established slow-channel mutation without shared haplotype with a European American patient

εp.Thr284Pro in the M2 domain of the ε subunit was identical to the first characterized slow-channel mutation reported in a patient of Swiss and Turkish descent [22]. We asked if the mutation in Pt. 4 derived from the same founder allele as the first reported patient. Therefore we sequenced exon 8 and its flanking intronic regions where nine SNPs were located (Fig. 1C). This revealed that the mutant allele in the Japanese patient had 'C', whereas the mutant allele in the European American patient had 'G' at rs12942540 in intron 8, which was located 82 nt. downstream of εp.Thr284Pro. Accordingly, εp.Thr284Pro in both patients is likely to have occurred independently in two ethnic groups.

3.5. δp.Arg44Trp and εp.Leu304Arg, but not βp.Met465Thr, decrease cell surface expression of AChR in transfected HEK293 cells

We next analyzed the effects of AChR expression of the remaining three mutations of δp.Arg44Trp, εp.Leu304Arg and βp.Met465Thr. We introduced wild-type or mutant α, β, δ, and ε subunit cDNAs along with EGFP cDNA into HEK293 cells (Fig. 2A), and measured cell surface expression of AChR detected by Alexa 647-labeled α-bungarotoxin using FACS. Expression of βp.Met465Thr-AChR was similar to that of wild-type AChR, whereas δp.Arg44Trp and εp.Leu304Arg markedly attenuated the cell surface expression of AChR (Figs. 2B and C). Accordingly, δp.Arg44Trp and εp.Leu304Arg cause endplate AChR deficiency.

3.6. βp.Met465Thr mildly shortens channel opening events, but not as much as the other established fast channel mutations

As βp.Met465Thr-AChR was efficiently expressed on HEK293 cells, we next recorded opening and closing of single AChR channels at limiting low concentrations of ACh by the patch clamp method (Fig. 3A). We found that the major burst duration (τ_3) was decreased from 3.31 ms to 1.93 ms (58.3%) in βp.Met465Thr-AChR (Table 3), while the conductance of βp.Met465Thr-AChR was normal. Distributions of opening probabilities of the clusters generated by 10 μM or greater concentrations of ACh made single peaks for both wild-type and mutant AChRs. Thus, βMet465Thr mildly shortens the channel openings but does not cause a mode switching in the kinetics of the receptor activation, which is seen in other FCCMS mutations [23,24].

3.7. A recessive mutation on the other allele in Pt. 3 remains unidentified

Functional prediction and characterization of the six mutations indicated that εp.Thr284Pro in Pt. 4 was a dominant slow-channel mutation [22], whereas the other five mutations in Pts. 1, 2, 3, and 5 were recessive loss-of-function mutations. The mutations in Pts. 1, 2, and 5 were biallelic, whereas a mutation was detected only on a single allele in Pt. 3 (Fig. 1C).

Please cite this article in press as: Yoshiteru Azuma, et al., Congenital myasthenic syndrome in Japan: Ethnically unique mutations in muscle nicotinic acetylcholine receptor subunits, Neuromuscular Disorders (2014), doi: 10.1016/j.nmd.2014.09.002

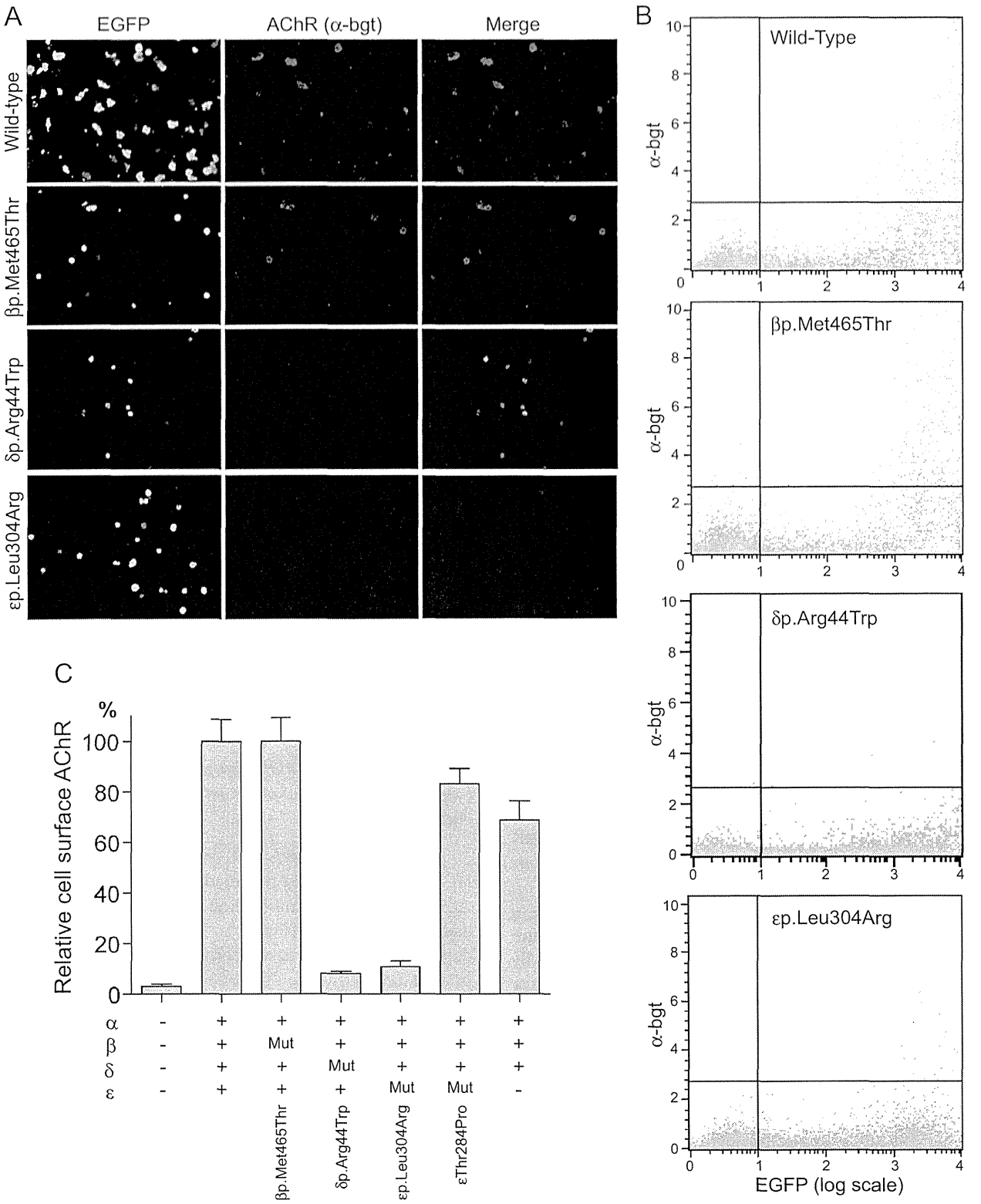

Fig. 2. Quantification of cell surface expression of wild-type and mutant AChRs on HEK293 cells. (A) HEK293 cells are transfected with wild-type or mutant AChR subunit cDNAs along with EGFP cDNA. Only transfected cells have EGFP signals and AChRs that are visualized with Alexa 647-labeled α-bungarotoxin (bgt). εp.Leu304Arg-AChR has less signals for AChRs compared to wild-type and βp.Met465Thr-AChRs. (B) Representative FACS profiles of EGFP and Alexa 647-labeled α-bgt. Both axes are shown in arbitrary units. The number of cells fractioned into the upper right quadrant is counted as AChR-positive cells. (C) Ratios of AChR-positive cells (the upper right quadrant) divided by EGFP-positive cells (the lower right quadrant). δp.Arg44Trp and εp.Leu304Arg markedly decrease AChR expression, whereas βp.Met465Thr and εp.Thr284Pro have no effect on AChR expression. ε-deficient $\alpha_2\beta\delta_2$-AChR are expressed at ~70% of wild-type, as we reported previously [21]. Mut, a mutant AChR subunit. Mean and SE are indicated ($n = 12$).

Please cite this article in press as: Yoshiteru Azuma, et al., Congenital myasthenic syndrome in Japan: Ethnically unique mutations in muscle nicotinic acetylcholine receptor subunits, Neuromuscular Disorders (2014), doi: 10.1016/j.nmd.2014.09.002

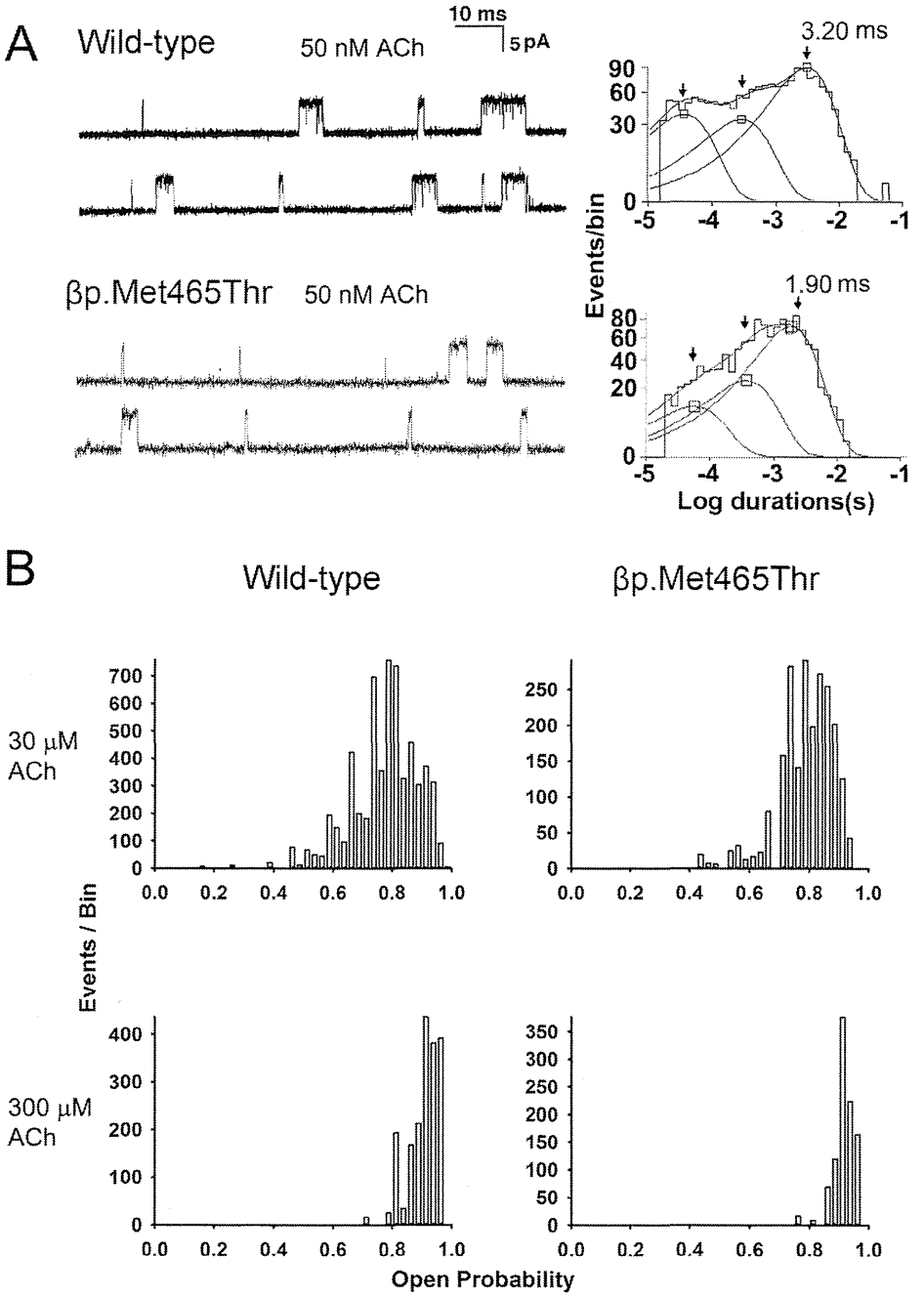

Fig. 3. Single channel currents of wild-type and mutant AChRs on HEK293 cells. (A) Left: Representative channel openings shown as upward deflections. Right: Burst duration histograms fitted to the sum of exponentials. Arrows indicate mean durations of dominant burst components. (B) Distribution of open probabilities from individual clusters obtained at the indicated ACh concentrations. Note that both wild-type and mutant AChRs make a single peak.

We scrutinized all exonic nucleotides in *CHRNE* in Pt. 3 by bidirectional sequencing, but detected none. We therefore hypothesized that a mutation on the other alleles was either a promoter mutation, a splice-site mutation disrupting a deep intronic splicing *cis*-element, or a large-scale DNA rearrangement. Sequencing of ~1 kb upstream of the translation initiation sites, however, revealed no mutation. We further analyzed genomic DNA by mate-pair sequencing of the whole genome. A total of 57 reads were mapped to *CHRNE*. Visual inspection of these reads, however, failed to detect any large-scale DNA rearrangements or any mutations. A recessive mutation on the other allele in *CHRNE* in Pt. 3 thus remains unidentified. We also analyzed 18 other CMS-causing genes using the mate-pair sequencing data in Pt. 3. As the mate-pair sequencing was for detecting a large-scale DNA rearrangement, the 18 genes were covered by only 10,116 reads. Although the coverage was not high enough for detecting SNVs, no candidate mutations were detected in Pt. 3.

Please cite this article in press as: Yoshiteru Azuma, et al., Congenital myasthenic syndrome in Japan: Ethnically unique mutations in muscle nicotinic acetylcholine receptor subunits. Neuromuscular Disorders (2014), doi: 10.1016/j.nmd.2014.09.002

Table 4
Fifteen previously reported FCCMS mutations and the currently analyzed βp.Met462Thr polymorphism.

Mutation	Burst duration (ms)			Expression	Domain	Reference
	Wild-type	Mutant	Ratio	(%)		
αp.Val152Leu (αV132L)	3.31	0.50	0.151	135	Extracellular domain of α	[25]
αp.Val208Met (αV188M)	3.31	0.68	0.205	90	Extracellular domain of α	[26]
αp.Phe276Leu (αF256L)	3.62	0.30	0.083	102	M2 domain of α	[27]
αp.Val305Ile (αV285I)	2.99	0.34	0.114	116	M3 domain of α	[28]
δp.Leu63Pro (δL42P)	3.31	0.18	0.054	37	Extracellular domain of δ	[14]
δp.Glu80Lys (δE59K)	5.06	2.75	0.543	62	Extracellular domain of δ	[29]
δp.Pro271Gln (δP250Q)	3.31	1.54	0.465	60	M1 domain of δ	[30]
εp.Thr58Lys (εT38K)	5.86	0.06	0.010	78	Extracellular domain of ε	[31]
εp.Trp75Arg (εW55R)	3.31	0.37	0.112	86	Extracellular domain of ε	[32]
εp.Pro141Leu (εP121L)	2.99	0.45	0.151	102	Extracellular domain of ε	[13]
εp.Asp195Asn (εD175N)	2.13	0.49	0.230	117[b]	Extracellular domain of ε	[33]
εp.Asn202Tyr (εN182Y)	2.13	0.65	0.305	117[b]	Extracellular domain of ε	[33]
εp.Ser433_Glu438dup (ε1254ins18)	2.80	1.01	0.361	47	Long cytoplasmic loop of ε	[23]
εp.Ala431Pro (εA411P)	n.a.[a]	n.a.[a]	n.a.[a]	31	Long cytoplasmic loop of ε	[24]
εp.Asn456del (εN436del)	3.31	1.24	0.375	51	Long cytoplasmic loop of ε	[34]
βp.Met462Thr (βM442T)	3.31	1.93	0.583	99	Long cytoplasmic loop of β	Current study

A major component of burst durations of wild-type and mutant AChRs expressed in HEK293 cells is indicated. Cell surface expression in HEK293 cells is normalized to that of wild-type. Channel openings are elicited by 50–100 nM ACh. Mutations in parentheses are legacy annotations used in original reports.

[a] Detailed ion channel kinetics are analyzed using a hidden Markov model, but burst durations are not indicated.

[b] Cell surface expression of recombinant AChR is not indicated, and the expression ratio is calculated from α-bungarotoxin binding sites of control and patient endplates.

4. Discussion

We identified six mutations in AChR subunit genes in five Japanese patients with CMS. We initially assumed that βp.Met465Thr in Pt. 6 was a mild fast-channel mutation. However, expansion of the SNP database later disclosed that βp.Met465Thr is a polymorphism that is frequently observed in the Japanese population. Fifteen previously reported FCCMS mutations shorten burst durations to 22.6 ± 16.1% of wild-type (mean and SD; range 1.0%–54.3%) (Table 4). A FCCMS mutation, δp.Glu80Lys (δE59K), decreases burst durations to 54.3% of wild-type [29], which is similar to 58.3% observed in the current βp.Met465Thr polymorphism. However, in contrast to βp.Met465Thr, δp.Glu80Lys reduces cell surface expression of AChR to 62% of wild-type [29]. Similarly, δp.Pro271Gln (δP250Q) mildly reduces burst durations to 46.5% of wild-type, but again, unlike βp.Met465Thr, this mutation reduces cell surface expression of AChR to 60% of wild-type [30]. A plot of normalized burst durations and normalized cell surface expressions suggests that a mean burst duration of less than ~30% causes FCCMS even when it does not affect the cell surface expression of AChR (Fig. 4). In contrast, a mean burst duration of between ~30% and ~60% causes FCCMS when the mutation reduces the cell surface expression of AChR to ~60% or less (Fig. 4). However, as no individual is homozygous for βp.Met465Thr or carries a null mutation on the other allele, pathogenicity of βp.Met465Thr in the absence of a normal *CHRND* on the other allele still remains unknown.

δp.Arg44Trp is close to the N-terminal end of the extracellular region (Fig. 5). We previously reported that a similar εp.Arg40Trp also causes AChR deficiency [35]. The specific function of this region, however, is not well dissected. εp.Leu304Arg is in the short extracellular link between the M2 and M3 transmembrane domains (Fig. 5). The functions of this link are not well characterized. In this link, only αp.Ser289Ile (αS269I) is reported in SCCMS [38]. βp.Met465Thr is located close to the C-terminal end of the long cytoplasmic loop that links the M3 and M4 transmembrane domains (Fig. 5). Interestingly, three FCCMS mutations in the long cytoplasmic loop are clustered close to the C-terminal end of the ε subunit [23,24,34,36,37], and similarly destabilize the channel open state. Two FCCMS mutations in this region, εp.Ser433_Glu438dup (ε1254ins18) [23] and εp.Ala431Pro (εA411P) [24], disrupt the fidelity of gating and result in unstable channel kinetics. In addition, another FCCMS

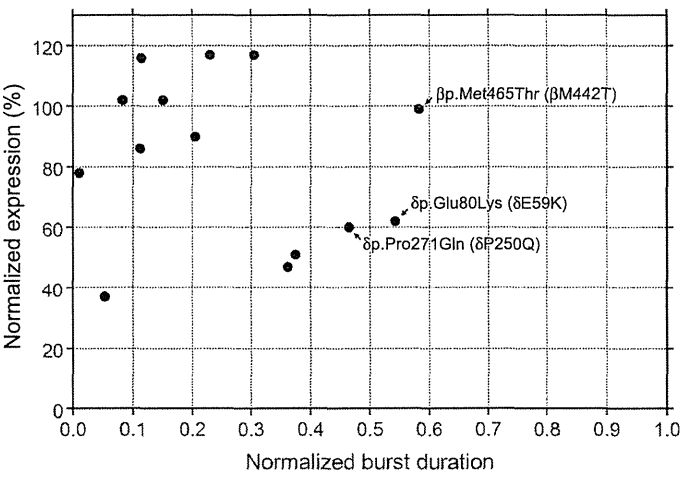

Fig. 4. Normalized burst durations and normalized cell surface expressions of previously reported FCCMS mutations and the currently analyzed βp.Met462Thr polymorphism shown in Table 4. Arrows point to mutations and a polymorphism that are addressed in the discussion.

Please cite this article in press as: Yoshiteru Azuma, et al., Congenital myasthenic syndrome in Japan: Ethnically unique mutations in muscle nicotinic acetylcholine receptor subunits, Neuromuscular Disorders (2014), doi: 10.1016/j.nmd.2014.09.002

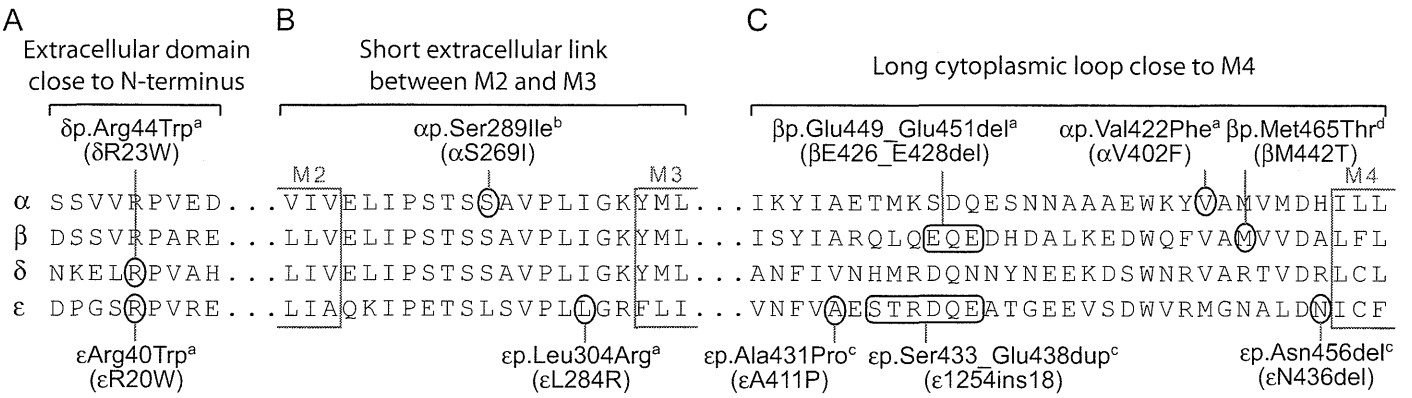

Fig. 5. Positions of the currently identified δp.Arg44Trp, εp.Leu304Arg and βp.Met465Thr, as well as previously reported CMS mutations. Mutations in the extracellular domain close the N-terminal end (A), the short extracellular link between the M2 and M3 transmembrane domains (B), and the long cytoplasmic loop close to the M4 transmembrane domain (C) are indicated. [a]δp.Arg44Trp (current report), εp.Arg40Trp [35], βp.Glu449_Glu451del [36], and αp.Val422Phe [37] cause AChR deficiency (AChR def.). [b]αp.Ser289Ile [38] causes SCCMS. [c]εp.Ala431Pro [24], ε p.Ser433_Glu438dup [23], and εp.Asn456del [34] cause FCCMS. [d]βp.Met465Thr is a currently analyzed polymorphism that shortens channel opening events. Mutations in parentheses are legacy annotations used in the original reports.

mutation in this region, εp.Asn456del (εN436del), destabilizes the diliganded receptor [34]. The C-terminal region of the long cytoplasmic loop of the ε subunit is thus likely to be crucial for stabilizing the open channel. In contrast to the three FCCMS mutations in the C-terminal end, however, βp.Met465Thr mildly shortens channel opening events and has no effect on the fidelity of channel gating, which may represent subunit-specificity and/or position-specificity of the amino acid substitutions.

Excluding δp.Arg44Trp that was previously reported in a healthy subject of unknown ethnicity [17], five of the six mutations in the AChR subunit genes in the current study and the five previously identified *COLQ* mutations [8] are unique to Japanese people. This is in contrast to some CMS mutations that are observed in unrelated families in Western and Middle Eastern countries. Especially, founder effects are implicated in two mutations: p.Asn88Lys in *RAPSN* [9–11] and c.1124_1127dupTGCC in *DOK7* [12]. CMS mutations are all recessively inherited except for those causing SCCMS. As heterozygous carriers of recessive CMS mutations exhibit no clinical phenotypes even by detailed electrophysiological studies, an asymptomatic carrier of a recessive CMS mutation has no disadvantage in transmitting the mutant allele to offspring. Lack of founder effects between the Japanese patients and patients of other nationalities thus suggest that most but not all CMS mutations arose *de novo* in a recent human history or in each family.

Acknowledgments

This study was supported by Grants-in-Aid from the MEXT and MHLW of Japan to KO. We would like to thank Dr. Andrew G. Engel for critical and constructive discussion on this project.

References

[1] Borges LS, Yechikhov S, Lee YI, et al. Identification of a motif in the acetylcholine receptor beta subunit whose phosphorylation regulates rapsyn association and postsynaptic receptor localization. J Neurosci 2008;28:11468–76.
[2] Bezakova G, Ruegg MA. New insights into the roles of agrin. Nat Rev Mol Cell Biol 2003;4:295–308.
[3] Budnik V, Salinas PC. Wnt signaling during synaptic development and plasticity. Curr Opin Neurobiol 2011;21:151–9.
[4] Korkut C, Budnik V. WNTs tune up the neuromuscular junction. Nat Rev Neurosci 2009;10:627–34.
[5] Ohno K, Ito M, Engel AG. Congenital myasthenic syndromes – molecular bases of congenital defects of proteins at the neuromuscular junction. In: Zaher A, editor. Neuromuscul. Disord. Rijeka: InTech; 2012. p. 175–200.
[6] Croxen R, Hatton C, Shelley C, et al. Recessive inheritance and variable penetrance of slow-channel congenital myasthenic syndromes. Neurology 2002;59:162–8.
[7] Ohno K, Engel AG, Brengman JM, et al. The spectrum of mutations causing endplate acetylcholinesterase deficiency. Ann Neurol 2000;47:162–70.
[8] Nakata T, Ito M, Azuma Y, et al. Mutations in the C-terminal domain of ColQ in endplate acetylcholinesterase deficiency compromise ColQ-MuSK interaction. Hum Mutat 2013;34:997–1004.
[9] Ohno K, Engel AG. Lack of founder haplotype for the rapsyn N88K mutation: N88K is an ancient founder mutation or arises from multiple founders. J Med Genet 2004;41:e8.
[10] Muller JS, Abicht A, Burke G, et al. The congenital myasthenic syndrome mutation RAPSN N88K derives from an ancient Indo-European founder. J Med Genet 2004;41:e104.
[11] Dunne V, Maselli RA. Common founder effect of rapsyn N88K studied using intragenic markers. J Hum Genet 2004;49:366–9.
[12] Ben Ammar A, Petit F, Alexandri N, et al. Phenotype genotype analysis in 15 patients presenting a congenital myasthenic syndrome due to mutations in DOK7. J Neurol 2010;257:754–66.
[13] Ohno K, Wang HL, Milone M, et al. Congenital myasthenic syndrome caused by decreased agonist binding affinity due to a mutation in the acetylcholine receptor epsilon subunit. Neuron 1996;17:157–70.
[14] Shen XM, Fukuda T, Ohno K, Sine SM, Engel AG. Congenital myasthenia-related AChR delta subunit mutation interferes with intersubunit communication essential for channel gating. J Clin Invest 2008;118:1867–76.
[15] Ishigaki K, Murakami T, Ito Y, et al. [Treatment approach to congenital myasthenic syndrome in a patient with acetylcholine receptor deficiency]. No to Hattatsu 2009;41:37–42.
[16] Irahara K, Komaki H, Honda R, et al. [Clinical features of congenital myasthenic syndrome in Japan]. No to Hattatsu 2012;44:450–4.
[17] Denning L, Anderson JA, Davis R, Gregg JP, Kuzdenyi J, Maselli RA. High throughput genetic analysis of congenital myasthenic syndromes using resequencing microarrays. PLoS ONE 2007;2:e918.

Please cite this article in press as: Yoshiteru Azuma, et al., Congenital myasthenic syndrome in Japan: Ethnically unique mutations in muscle nicotinic acetylcholine receptor subunits, Neuromuscular Disorders (2014), doi: 10.1016/j.nmd.2014.09.002

[18] Narahara M, Higasa K, Nakamura S, et al. Large-scale East-Asian eQTL mapping reveals novel candidate genes for LD mapping and the genomic landscape of transcriptional effects of sequence variants. PLoS ONE 2014;9:e100924.
[19] Engel AG, Ohno K, Bouzat C, Sine SM, Griggs RC. End-plate acetylcholine receptor deficiency due to nonsense mutations in the epsilon subunit. Ann Neurol 1996;40:810–17.
[20] Engel AG, Ohno K, Milone M, et al. New mutations in acetylcholine receptor subunit genes reveal heterogeneity in the slow-channel congenital myasthenic syndrome. Hum Mol Genet 1996;5:1217–27.
[21] Ohno K, Quiram PA, Milone M, et al. Congenital myasthenic syndromes due to heteroallelic nonsense/missense mutations in the acetylcholine receptor epsilon subunit gene: identification and functional characterization of six new mutations. Hum Mol Genet 1997;6:753–66.
[22] Ohno K, Hutchinson DO, Milone M, et al. Congenital myasthenic syndrome caused by prolonged acetylcholine receptor channel openings due to a mutation in the M2 domain of the epsilon subunit. Proc Natl Acad Sci U S A 1995;92:758–62.
[23] Milone M, Wang H-L, Ohno K, et al. Mode switching kinetics produced by a naturally occurring mutation in the cytoplasmic loop of the human acetylcholine receptor epsilon subunit. Neuron 1998;20:575–88.
[24] Wang H-L, Ohno K, Milone M, et al. Fundamental gating mechanism of nicotinic receptor channel revealed by mutation causing a congenital myasthenic syndrome. J Gen Physiol 2000;116:449–62.
[25] Shen X-M, Ohno K, Tsujino A, et al. Mutation causing severe myasthenia reveals functional asymmetry of AChR signature cystine loops in agonist binding and gating. J Clin Invest 2003;111:497–505.
[26] Shen XM, Brengman JM, Sine SM, Engel AG. Myasthenic syndrome AChRalpha C-loop mutant disrupts initiation of channel gating. J Clin Invest 2012;122:2613–21.
[27] Webster R, Brydson M, Croxen R, Newsom-Davis J, Vincent A, Beeson D. Mutation in the AChR ion channel gate underlies a fast channel congenital myasthenic syndrome. Neurology 2004;62:1090–6.
[28] Wang H-L, Milone M, Ohno K, et al. Acetylcholine receptor M3 domain: stereochemical and volume contributions to channel gating. Nat Neurosci 1999;2:226–33.
[29] Brownlow S, Webster R, Croxen R, et al. Acetylcholine receptor d subunit mutations underlie a fast-channel myasthenic syndrome and arthrogryposis multiplex congenita. J Clin Invest 2001;108:125–30.
[30] Shen XM, Ohno K, Fukudome T, et al. Congenital myasthenic syndrome caused by low-expressor fast-channel AChR delta subunit mutation. Neurology 2002;59:1881–8.
[31] Webster R, Liu WW, Chaouch A, Lochmuller H, Beeson D. Fast-channel congenital myasthenic syndrome with a novel acetylcholine receptor mutation at the alpha-epsilon subunit interface. Neuromuscul Disord 2014;24:143–7.
[32] Shen XM, Brengman JM, Edvardson S, Sine SM, Engel AG. Highly fatal fast-channel syndrome caused by AChR epsilon subunit mutation at the agonist binding site. Neurology 2012;79:449–54.
[33] Sine SM, Shen X-M, Wang H-L, et al. Naturally occurring mutations at the acetylcholine receptor binding site independently alter ACh binding and channel gating. J Gen Physiol 2002;120:483–96.
[34] Shen XM, Ohno K, Sine SM, Engel AG. Subunit-specific contribution to agonist binding and channel gating revealed by inherited mutation in muscle acetylcholine receptor M3-M4 linker. Brain 2005;128:345–55.
[35] Shen X-M, Ohno K, Milone M, Brengman JM, Spilsbury P, Engel AG Low-affinity fast-channel syndrome. Neurology 2001;56(Suppl. 3):A60. (abstract).
[36] Quiram PA, Ohno K, Milone M, et al. Mutation causing congenital myasthenia reveals acetylcholine receptor beta/delta subunit interaction essential for assembly. J Clin Invest 1999;104:1403–10.
[37] Milone M, Shen X-M, Ohno K, et al. Unusual congenital myasthenic syndrome with endplate AChR deficiency caused by alpha subunit mutations and a remitting-relapsing clinical course. Neurology 1999;51(Suppl. 2):A185. (abstract).
[38] Croxen R, Newland C, Beeson D, et al. Mutations in different functional domains of the human muscle acetylcholine receptor alpha subunit in patients with the slow-channel congenital myasthenic syndrome. Hum Mol Genet 1997;6:767–74.

Please cite this article in press as: Yoshiteru Azuma, et al., Congenital myasthenic syndrome in Japan: Ethnically unique mutations in muscle nicotinic acetylcholine receptor subunits, Neuromuscular Disorders (2014), doi: 10.1016/j.nmd.2014.09.002